

AFIT/GA/ENY/91D-12

1

AD-A243 891



DTIC
ELECTE
JAN 06 1992
S D D

**THRUST VECTOR CONTROL OF AN
OVEREXPANDED SUPERSONIC NOZZLE USING
PIN INSERTION AND ROTATING AIRFOILS**

THESIS

Curtis R. Ambler
Captain, USAF

AFIT/GA/ENY/91D-12

Approved for public release; distribution unlimited

92-00057



92 7 12

AFIT/OA/ENY/91D-12

THRUST VECTOR CONTROL OF AN
OVEREXPANDED SUPERSONIC NOZZLE USING
PIN INSERTION AND ROTATING AIRFOILS

THIS IS

Presented to the Faculty of the School of Engineering
of the Air Force Institute of Technology
Air University
In Partial Fulfillment of the
Requirements for the Degree of
Master of Science in Astronautical Engineering

Curtis R. Ambler

Captain, USAF

December 1991

Approved for public release; distribution unlimited

A-1

Preface

I have examined the performance of probe thrust vector control of a conical nozzle and a conical nozzle with a confined jet attachment. The objective was to gather data that would aid in the evaluation of thrust vector control mechanisms for nozzle applications.

I would like to thank my thesis advisor, Dr. M.E. Franke, for his encouragement and guidance during my experiments. The support of my thesis committee, Dr. W.C. Elrod and Capt John Doty, was invaluable.

The AFIT technical and model fabrication support was excellent. Special thanks to Mr. Jay Anderson whose efforts enabled the data acquisition and control software necessary to accomplish this study to work effectively. Special thanks to Mr Dave Driscoll who was always there to lend his expertise and work with me when special fabrication requirements came up.

Finally, very special thanks to my new wife Laura. Who was able to love and support me through this research effort.

Curtis R. Amble

Table of Contents

	<u>Page</u>
Preface	ii
List of Figures	v
List of Tables	vii
List of Symbols	viii
Abstract	ix
I. Introduction1
A. Background.1
B. Objectives.5
C. Approach.5
II. Experimental Apparatus7
A. Test Stand.7
B. High Pressure Air Supply.7
1.Primary Air.7
2.Secondary Air.9
C. Test Article.9
1.Conical Nozzle9
2.Confined Jet Attachment..12
3.Probes13
4.Cylindrical Pin Insertion Assembly.13
5.Double Wedge Airfoil Orientation.16
D. Test Control and Instrumentation.19
1.Force Balance24
2.Pressure Measurements..26
3.Data Processing.27
III. Experimental Procedure28
A. General28
B. Data Acquisition.29
C. Steady State Axial Runs31
D. Steady State Vectored Runs.31
E. Vector Transient Runs31

IV.	Test Results and Discussion.33
	A. Axial Operation33
	B. Vectored Operation.42
	1. Cylindrical Pins in Conical Nozzle43
	2. Cylindrical Pins in Confined Jet46
	3. Double Wedge Airfoils as a Probe Thrust Vector Control Device.51
	C. Transient Response Data53
	1. Force Balance Frequency Response53
	2. Cylinder Wall Pressure Real Time Data.62
	3. Insertion System Repeatability65
	D. Probe Thrust Vector Control Transient Response of the Confined Jet Nozzle.66
	1. Insertion Response66
	2. Extraction Response.68
	E. Multiple Pins in the Confined Jet Nozzle.68
	F. Probe Thrust Vector Control Transient Response of the Conical Nozzle73
V.	Conclusions.75
VI.	Recommendations.79
	Bibliography126
	Vita127

List of Figures

<u>Figure</u>	<u>Page</u>
1. Axial and Vectored Operation of the Confined Jet Nozzle and Conical Nozzle.	4
2. Test Stand (schematic)	8
3. Test Article	10
4. Test Article (schematic)	11
5. Static Probes.	14
6. Pneumatic Cylinder (schematic)	15
7. Insertion/Extraction Assembly Installed on Confined Jet Nozzle	17
8. Pneumatic Insertion/Extraction Assembly.	18
9. Airfoil Orientation Assembly Installed on Confined Jet Nozzle	20
10. Airfoil Orientation Assembly	21
11. Test Control/Instrumentation (schematic)	23
12. Force Balance.	25
13. Conical Nozzle Flow Condition at Static Pressure Tap Locations.	34
14. Conical Nozzle Flow Condition at Static Pressure Tap Locations for Various Plenum Pressures	35
15. Confined Jet Flow Condition at Static Pressure Tap Locations.	36
16. Confined Jet Flow Condition at Static Pressure Tap Locations for Various Plenum Pressures	37
17. Area Ratio for Conical Nozzle (AR _{cn}) and Confined Jet Nozzle (AR _{cj}) for Axial Locations in the Nozzle Section.	39

18.	Nondimensional Axial Force vs Plenum Pressure for Various Test Configurations.	41
19.	Conical Nozzle NDFa vs Pp for Various PDs.	44
20.	Conical Nozzle NDFl vs Pp for Various PDs.	45
21.	Conical Nozzle Force Ratio (Fl/Fa) vs Pp for Various PDs.	47
22.	Confined Jet NDFa vs Pp for Various PDs.	49
23.	Confined Jet NDFl vs Pp for Various PDs.	50
24.	Confined Jet Force Ratio (Fl/Fa) vs Pp for Various PDs.	52
25.	Axial Force Transducer Natural Frequency Distribution	55
26.	Lateral Force Transducer Natural Frequency Distribution	56
27.	Steady State Axial Force Balance Frequency Distribution	58
28.	Steady State Axial Real Time Force Data of Confined Jet Nozzle.	59
29.	Steady State Vectored Force Balance Frequency Distributions of Confined Jet Nozzle.	60
30.	Steady State Vectored Real Time Force Data of Confined Jet Nozzle	61
31.	Pin Insertion Real Time Confined Jet Nozzle Cylinder Wall Pressure Data	63
32.	Pin Extraction Real Time Confined Jet Nozzle Cylinder Wall Pressure Data	64
33.	Pin Insertion Real Time Force Data/Flow Attachment to Pin.	67
34.	Pin Extraction, Cylinder Wall Pressure Data/Abrupt Transition.	69
35.	Pin Extraction, Cylinder Wall Pressure Data/Transition with Hysteresis	70

36.	Pin Extraction, Cylinder Wall Pressure Data/Unstable Transition	71
-----	--	----

List of Tables

<u>Table</u>	<u>Page</u>
1. Conical Nozzle Dimensions	12
2. Confined Jet Attachment Dimensions.	13
3. Axial Location of Separation Point in Conical Nozzle	40
4. Axial Location of Separation Point in Confined Jet Nozzle	41

List of Symbols

Symbol Definition

Aa	Area of Conical Nozzle at Axial Location
AD	Airfoil Insertion Depth (in)
Ae	Conical Nozzle Exit Area
Aec	Confined Jet End Capt Exit Area
ARcj	Confined Jet Area Ratio
ARcn	Conical Nozzle Area Ratio
As	Area of Conical Nozzle at Separation Point
At	Area of the Conical Nozzle Throat
Fa	Measured Axial Force (lbf)
F _l	Measured Lateral Force (lbf)
NDFa	Nondimensional Axial Force, $F_a/(P_p A_t)$
NDF _l	Nondimensional Lateral Force, $F_l/(P_p A_t)$
La	Axial Distance from Edge of the Nozzle Throat (in)
Ls	Axial Distance from Separation Point to Throat (in)
Pcjc	Static Pressure at the Confined Jet Cylinder Wall (psig)
PD	Pin Insertion Depth (in)
Pp	Primary Air Plenum Pressure (psia)
Pw	Static Pressure at the Conical Nozzle Wall (psia)

Abstract

An experimental study of probe thrust vector control of overexpanded supersonic flow in nozzles using moveable probes as the vectoring mechanism is presented. Two types of moveable probes were used. The first inserted cylindrical probes through the wall of the nozzle to set depths relative to the nozzle wall. The second used rotating airfoils, inserted within the nozzle flow, rotated to various angles of attack relative to the nozzle centerline. The effectiveness of these probe thrust vector control mechanisms were investigated for a confined jet and conical nozzle. The objective of this study was to evaluate performance and transient characteristics of these probe thrust vector control mechanisms.

Data are presented for both a confined jet nozzle and conical nozzle operating with primary stagnation pressures ranging from 150 psia to 460 psia and exhausting to atmospheric pressure. The range in pressure above 150 psia represents the region where flow in both configurations are stable and supersonic in axial operation. Limitations in the pressure supply allowed evaluation of both configurations only in the overexpanded flow regime. Axial force, lateral force, and static nozzle wall pressure distribution data were

measured for axial and vectored operation for each nozzle configuration. Parameters that were varied included primary stagnation pressure, cylinder insertion depth, airfoil insertion depth and angle of attack.

The test results showed that probe thrust vector control using cylindrical pin insertion is a viable thrust vectoring mechanism. The performance of the cylindrical pins was repeatable in both nozzle configurations. The lateral forces produced using cylindrical pin insertion compared favorably with previous studies using secondary air injection on the same nozzle configurations. The test results for the inserted airfoils showed that axial operation with inserted airfoils was not possible. The airfoils produced similar lateral forces as the cylindrical pins within the plane of the flow disturbance. However, the airfoils were not able to produce lateral forces out of the plane of the flow disturbance.

THRUST VECTOR CONTROL OF AN OVEREXPANDED
SUPERSONIC NOZZLE USING PIN INSERTION
AND ROTATING AIRFOILS

I. INTRODUCTION

A. Background

Conventional thrust vector control concepts for supersonic nozzles basically fall into two categories: mechanical and fluid dynamic. Mechanical thrust vector control is accomplished in two ways: gimbaling of the exhaust nozzle or deflecting the exhaust flow at the exit plane using moveable vanes or flaps. Fluid dynamic thrust vector control, uses gas (or liquid) injected at the nozzle wall. There are two types of fluid dynamic thrust vector control; secondary injection uses pressurized injectant and boundary layer uses ambient air outside the nozzle for the injectant. Both the mechanical and fluid dynamic thrust vector control concepts can have significant performance penalties associated with them.

Gimbaling and flow deflection systems are inherently complicated and require heavy mechanisms that result in a reduced payload capability. Flow deflection systems can have

an additional thrust loss if the mechanism is constantly exposed to the exhaust flow. Secondary injection thrust vector control systems must carry enough consumable injectant to accomplish the vectoring objective. The additional weight in propellant can result in a significant payload penalty if a lot of maneuvering is required. Boundary layer thrust vector control systems are limited to lower altitudes where the ambient pressure is greater than the static pressure along the nozzle wall (1).

The moveable probe thrust vector control system is essentially a hybrid of mechanical and fluid dynamic thrust vector control systems. The probe thrust vector control system could use a variety of devices (pneumatic, hydraulic, or electromagnetic systems) to insert and extract the probe from the exhaust flow. This offers a significant reduction in weight over gimbaling, flow deflection, and secondary injection thrust vector control systems. The actuator mechanism is generally much smaller for typical mechanical thrust vector control systems. Cavalleri, Tiarn, and Ready (1) estimated an 80% reduction in weight for a comparable probe thrust vector control system for the solid rocket booster on the space shuttle versus the current gimbaling system in use. The probe thrust vector control system also offers a possible weight advantage over secondary injection

thrust vector control designs with the elimination of injectant storage tanks.

The governing concept for internal nozzle (inter-nozzle) vectoring for the probe thrust vector control and secondary injection thrust vector control systems is essentially the same. The axial and vectored operation of the conical nozzle and confined jet nozzle are presented in Figure 1. A disturbance (pin or injectant stream) is generated in the expanding flow along one side of the nozzle wall. This disturbance generates a bow shock upstream of the disturbance which generates a separated region downstream of the bow shock. The separated region on one side of the nozzle wall creates a pressure imbalance on the other side of the nozzle plane. This pressure imbalance causes the expanding flow to attach itself to the side of the nozzle opposite the disturbance (1). The attached (or vectored) flow exits the nozzle along the nozzle wall; and in the case of the conical nozzle, at approximately the half angle of the nozzle.

The use of this type of thrust vector control in conical nozzles results in lateral forces of up to 25% of the axial thrust. The lateral forces are much smaller than those generated by gimbaling or external flow deflection. The addition of a confined jet section to the conical nozzle can increase the lateral forces generated by probe insertion and secondary injection thrust vector control by increasing the

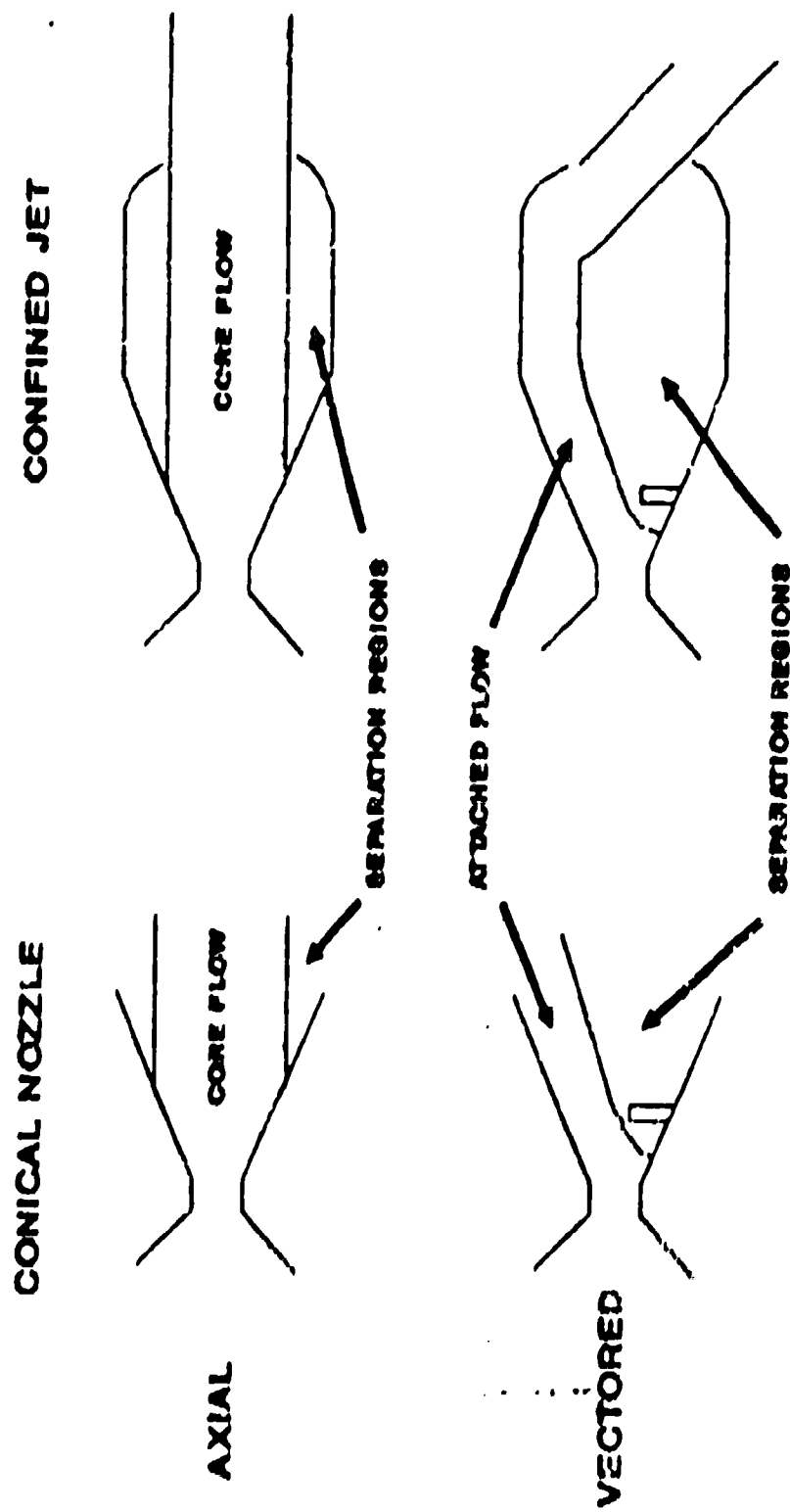


**FIGURE 1 AXIAL AND VECTORED OPERATION
OF THE CONFINED JET NOZZLE AND CONICAL NOZZLE**

turning angle of the attached flow as it exits the nozzle. The use of a confined jet can increase the lateral force generated to approximately 35-50% of the axial thrust.

Investigations by Fitzgerald and Kampe (2) identified design criteria for an axisymmetric confined jet using secondary air injection. This work was followed by several studies at the Air Force Institute of Technology (AFIT) by Porzio (5), Friddell (3), and Herup (4). The majority of the AFIT studies concentrated on secondary injection as the vectoring mechanism. The only work at AFIT using probe thrust vector control in a confined jet was that of Herup (4) in 1989. Herup found in static tests that cylindrical pins inserted in the nozzle and airfoils inserted and rotated at an angle of attack relative to the nozzle centerline offered possible alternatives to secondary injection as a thrust vector control mechanism.

B. Objectives

The overall objective of this study was to characterize the performance and the transient from axial to vectored operation of a confined jet nozzle and a conical nozzle using probe thrust vector control as the vectoring mechanism. This required the development of an acceptable dynamic insertion design for the cylindrical pins and the airfoils. The aspects of these will be discussed further in Section II.C. Test Article. Software was written to

simultaneously control the probe thrust vector control devices and acquire transient data.

The main objectives of this investigation were to:

- 1) Characterize the axial and vectored performance of the conical nozzle and confined jet nozzle using probe thrust vector control.
- 2) Compare performance data for these configurations with secondary injection thrust vector control.
- 3) Define the primary parameters and characterize the vector response time from axial to vectored operation for these configurations using probe thrust vector control devices.
- 4) Compare vector response time data for the confined jet nozzle using probe thrust vector control with transient studies using secondary injection thrust vector control.

C. Approach

The primary hurdles in this investigation were the development of acceptable dynamic probe thrust vector control hardware for pin insertion and airfoil orientation and the software to control the probe thrust vector control devices and collect data. The two nozzle configurations tested, conical nozzle and confined jet nozzle, were used in previous AFIT investigations. The same nozzles used in previous studies using secondary injection enabled a reasonable comparison of these probe thrust vector control mechanisms with secondary injection thrust vector control.

II Experimental Apparatus

A Test Stand

The nozzle test stand used in this study was originally developed by Porzio (5) in 1984. It is a blow-down facility that consists of a 12-inch diameter primary air plenum and a secondary air manifold. These are hung from a two degree of freedom pendulum. This allows the nozzle/plenum assembly to translate freely in the plane of the floor for small rotations of the plenum arm. This allows force measurements in the axial and lateral directions in the plane of the floor. A schematic of the nozzle test stand is presented as Figure 2.

B High Pressure Air Supply

High pressure air was supplied at room temperature at a pressure of approximately 2500 psia from a high pressure air system through a main cut-off valve outside the building.

1. Primary Air The high pressure air is fed to a manual control valve in line with two staging valves. The first stage valve steps down the air pressure and pressurizes the second stage valve. The second stage valve controls airflow to the primary air plenum. Both these valves are controlled electronically from the control room. The maximum pressure for the primary air is approximately 500 psig due to structural limits on the primary air plenum.

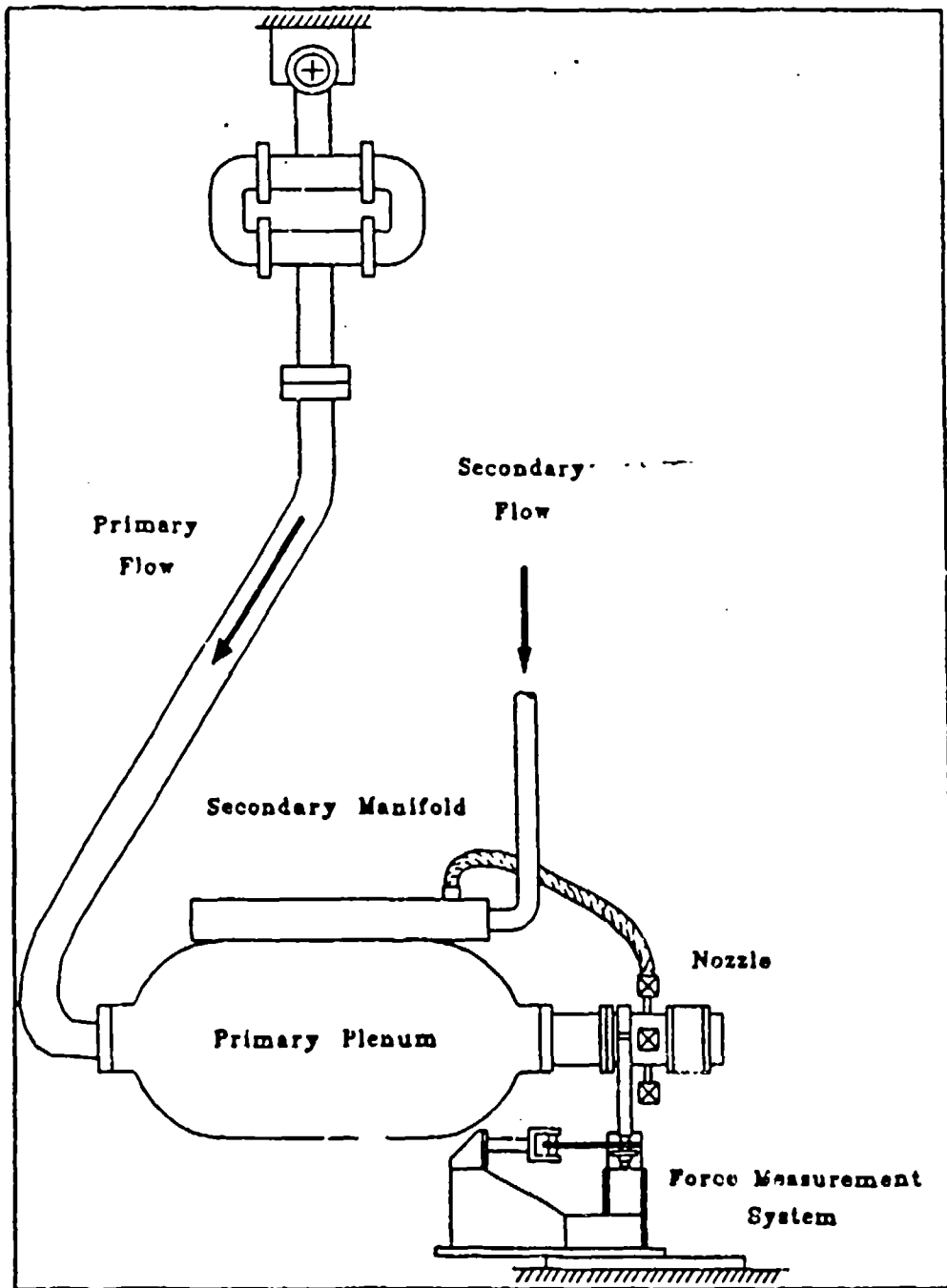


FIGURE 2 TEST STAND (SCHEMATIC) (4)

2. Secondary Air The secondary air is bled from the high pressure line upstream from the manual control valve on the primary air line. This feeds to a manual control valve that pressurizes a manually set staging valve. The manual staging valve allows the secondary manifold pressure to be set at pressures up to 350 psig from the control room.

C Test Article

The test article used in this study is shown in Figure 3 and a schematic diagram in Figure 4. The test article consists of four parts: an upstream 2.06 in diameter constant area section, an axisymmetric conical converging-diverging section with four 0.19 in diameter probe insertion ports, and the confined jet attachment. All nozzle parts were fabricated from aluminum and bolted together and sealed with "O" rings.

The upstream constant area section (not pictured) was required to allow installation of the force balance without interfering with the primary air plenum. The two axis force balance is bolted to this section upstream of the converging-diverging section. Installation of the force balance at this location simplified the installation of the probe insertion and airfoil orientation devices.

1. Conical Nozzle The converging-diverging section was originally fabricated for use in a confined jet

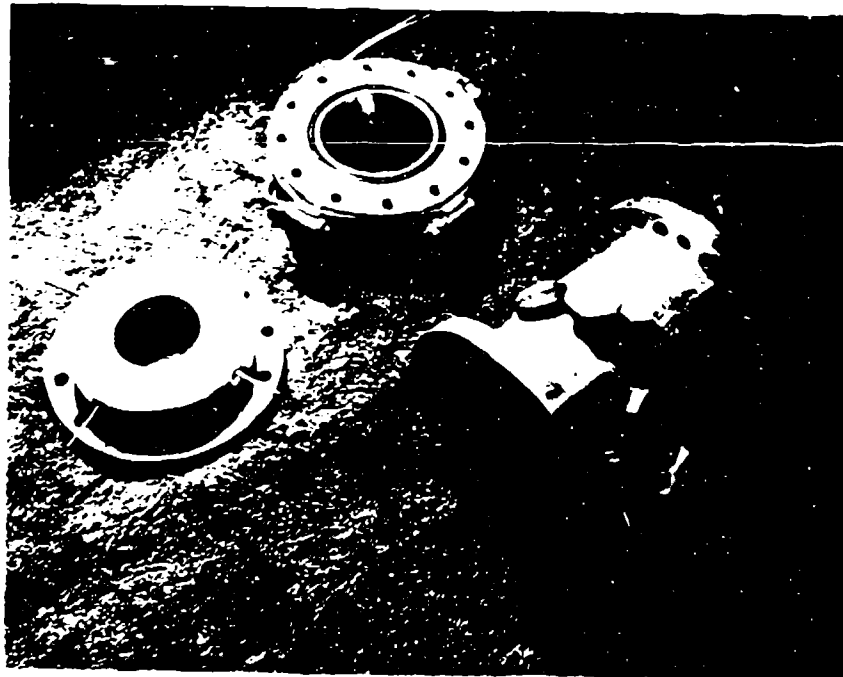


FIGURE 3 TEST ARTICLE

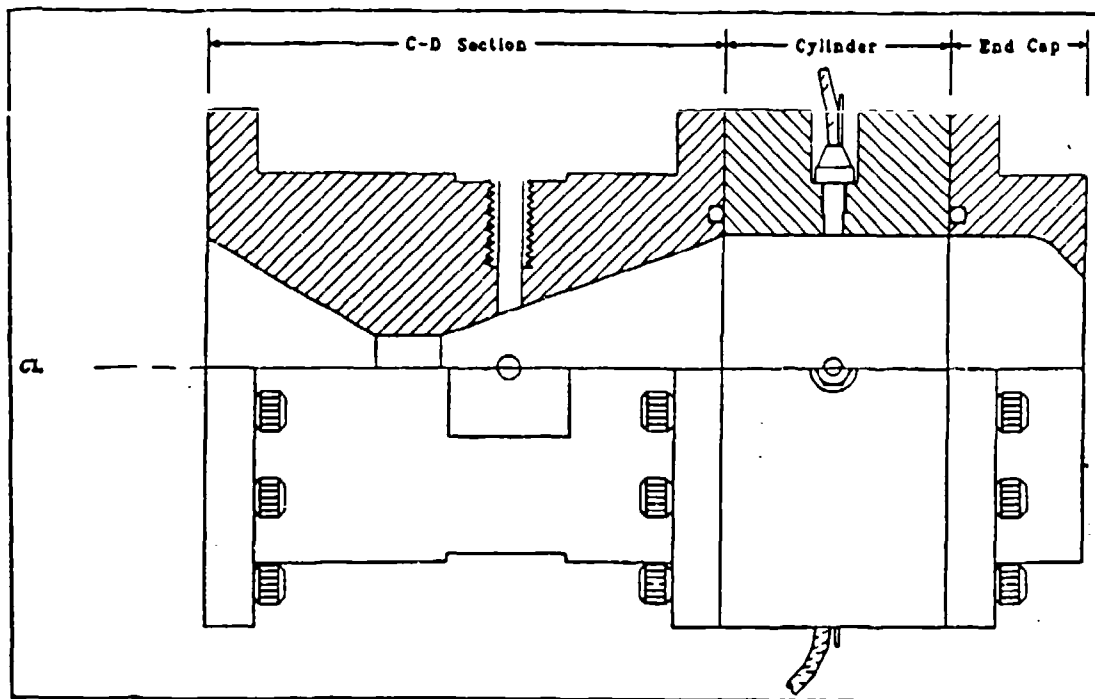


FIGURE 4 TEST ARTICLE (SCHEMATIC) (3)

arrangement. The diverging conical nozzle has a half angle and length sufficient to overexpand the air flow for the plenum pressure (P_p) ranges in this study. Twelve probe insertion ports were available at three axial locations along the nozzle in groups of four which were all spaced 90 deg apart radially. In this study the axial location used was located 0.47 in from the nozzle throat. Ten static pressure taps are located at 0.24 in intervals axially along the nozzle beginning at 0.71 in from the throat. The important nozzle dimensions are listed in Table 1 and presented visually in Figure 4.

TABLE 1
Conical Nozzle Dimensions

Throat Diameter	0.5 in
Exit Diameter	2.06 in
Area Ratio (A_e/A_t)	17:1
Conical Divergence Half Angle	19.7 deg
Conical Convergence Half Angle	37.3 deg
Throat Length	0.5 in
Probe Insertion Port Diameter	0.19 in
Probe Insertion Port Axial Location from Throat	0.44 in

2. Confined Jet Attachment The confined jet attachment consisted of two parts: a constant area cylinder and a converging end cap (see Figure 4). The constant area cylinder had four static pressure taps and four dynamic pressure taps machined into the wall 90 degrees apart at the center of the cylinder section. The inside of the end cap section is machined such that the exit lip is approximately

45 degrees. The end cap has four static taps located 90 degrees apart. The important dimensions for the confined jet attachment are listed in Table 2.

TABLE 2
Confined Jet Attachment Dimensions

Cylinder Diameter	2.06 in
Cylinder Length	1.75 in
End Cap Exit Diameter	1.40 in
Area Ratio (A_{ec}/A_t)	7.84
End Cap Reconvergence Angle	45 deg

3. Probes Two types of probes were used in this study: cylindrical pins and double wedge airfoils. The static probes used in this study are pictured in Figure 5. The diameter of the cylindrical pins were 0.188 inches in diameter, slightly smaller than the 0.19 in diameter of the insertion ports. The double wedge airfoils were diamond shaped in cross-section. The airfoil chord length (0.188 in) was equal to the cylindrical pin diameter and the thickness (0.06 in) was approximately 30% of the chord length. These dimensions were found by Herup (4) to vector the confined jet nozzle in static tests.

4. Cylindrical Pin Insertion Assembly The transient evaluation of probe thrust vector control using probe insertion and airfoil rotation presented an interesting design problem. The cylindrical pin insertion was fairly straight forward. Double acting 5/16 in pneumatic cylinders with a

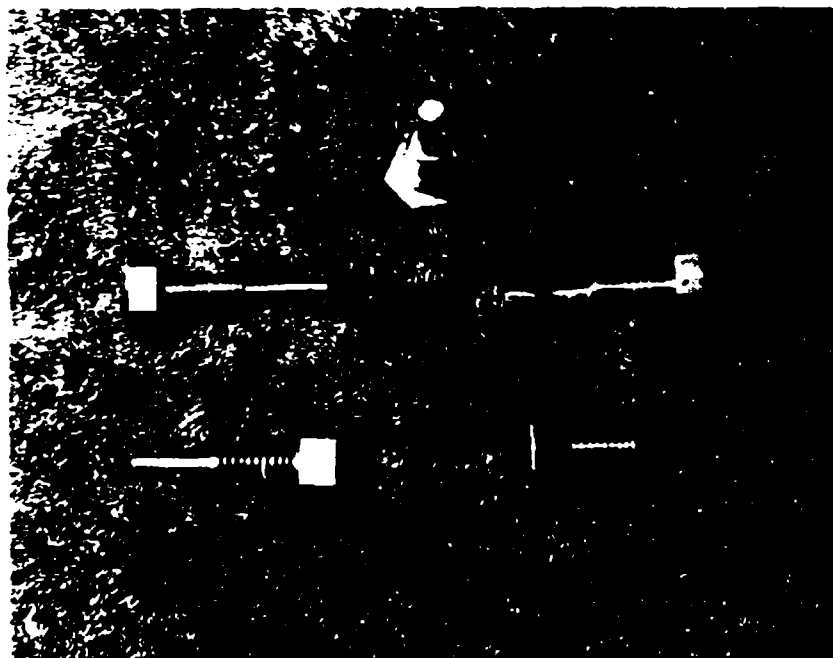


FIGURE 5 STATIC PROBES

1.0 in stroke length were selected as the insertion device and they were actuated by solenoid air valves. A schematic of the pneumatic cylinder is presented in Figure 6.

The installation of these cylinders on the nozzle insertion ports required a mounting adapter due to the existing 16 threads per in on the nozzle insertion ports and the 40 threads per inch on the pneumatic cylinders. Cylindrical tips, 0.188 in diameter, were made to thread on to the pneumatic cylinder. The cylindrical tips enabled the pin insertion depth to be set between 0.1 in and over 0.2 in using the threads on the pneumatic cylinder. Pin insertion depth is defined as the distance that the pin is inserted past the nozzle wall measured from the downstream side of the insertion port. Zero pin insertion depth corresponds to the probe thrust vector control device located flush with the downstream edge of the insertion port. The 1.0 in stroke on the pneumatic cylinders presented a problem. When the pneumatic cylinder was installed with the mounting adapter, the cylinder was withdrawn well past the nozzle wall leaving a cavity in the extracted position. Collars were made for the pneumatic cylinders that limited the cylinder stroke to withdraw the pin to just beyond the nozzle wall. The pneumatic cylindrical pin insertion assembly is shown installed on the confined jet nozzle in Figure 7. The pneumatic cylinder insertion assembly is shown assembled and

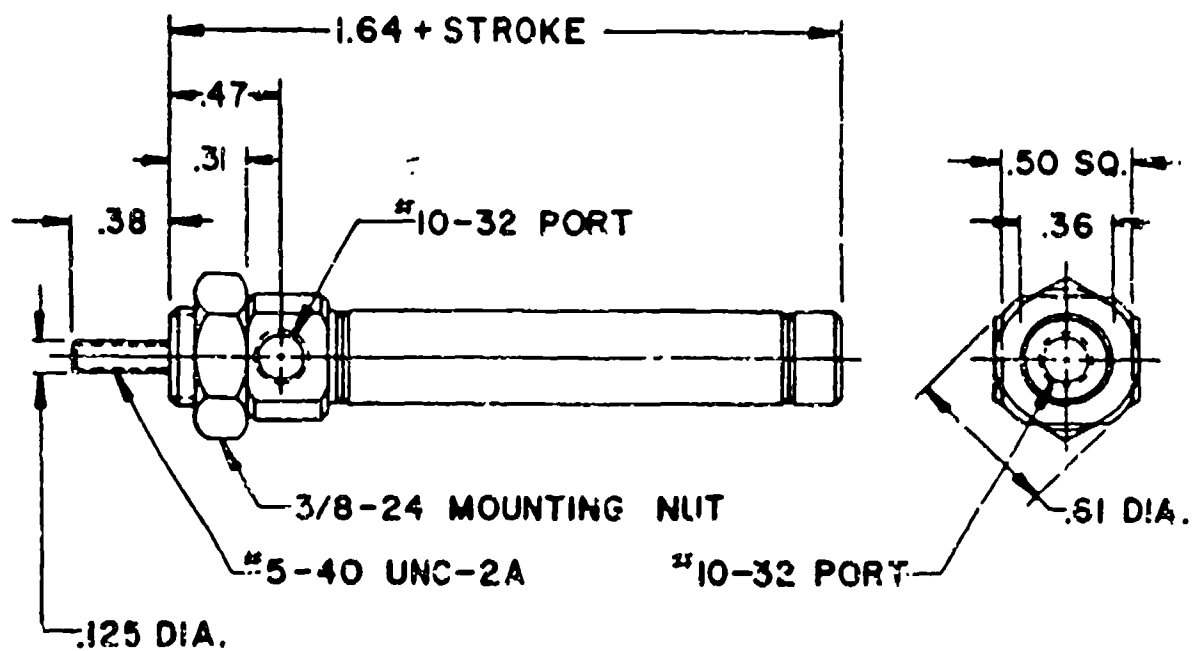
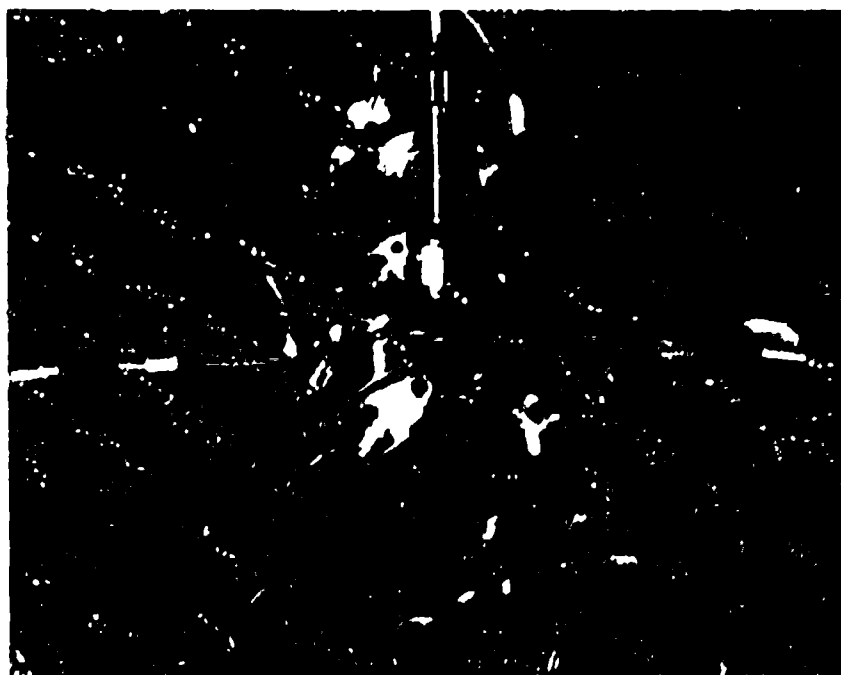


FIGURE 6 PNEUMATIC CYLINDER (SCHEMATIC)



**FIGURE 7 INSERTION/EXTRACTION ASSEMBLY
INSTALLED ON CONFINED JET NOZZLE**

disassembled in Figure 8. Adapters were made to attach Endevco pressure transducers to each end of the pneumatic cylinder. This enabled the time response of the air pressure applied to the pneumatic cylinders inserting and extracting the pins to be measured.

5. Double Wedge Airfoil Orientation It was impossible, due to time constraints, to obtain a device that would insert and orient the airfoils as part of this study. However, the results Herup (4) obtained indicated this was not necessary as he found axial airfoils inserted at zero degrees angle of attack relative to the nozzle centerline. This indicated that the flow could be vectored by rotating the airfoils between zero and 180 degrees angle of attack. The airfoil orientation assembly is shown installed on the nozzle in Figure 9 and disassembled in Figure 10. Two stepper motors were used that allowed the rotation to be commanded at various speeds from the control room. Airfoil rotation assemblies were made that threaded into the insertion ports and allowed the airfoils to rotate freely. This enabled the airfoil insertion depth to be set accurately and the airfoils rotated into position without changing the insertion depth. The rotation assemblies were connected by gears (1:1 gear ratio) to the DC stepper motors. This enabled the airfoil angle of attack to be commanded from the control room with an accuracy of less than one degree.

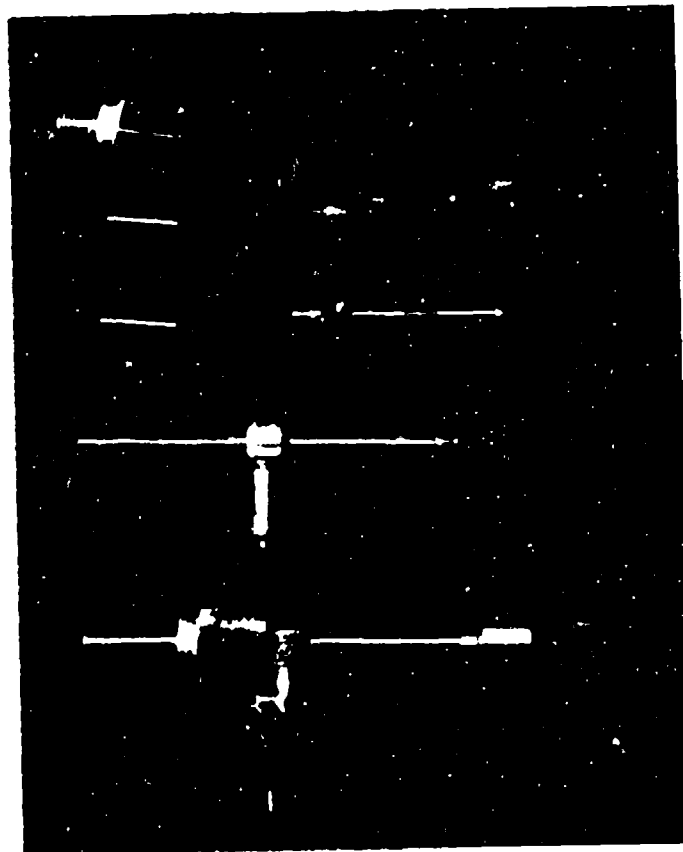


**FIGURE 8 PNEUMATIC
INSERTION/EXTRACTION ASSEMBLY**

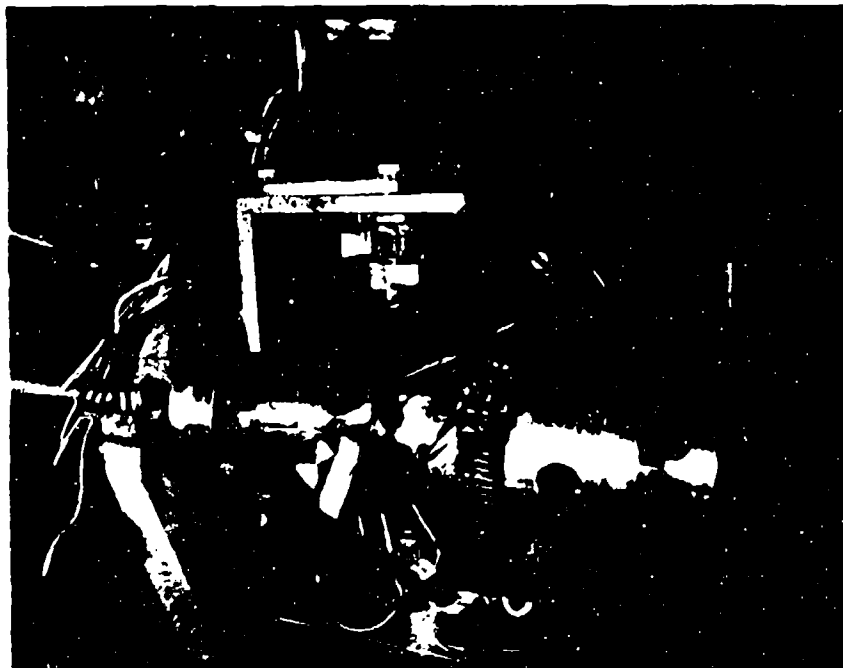


**FIGURE 9 AIRFOIL ORIENTATION ASSEMBLY
INSTALLED ON CONFINED JET NOZZLE**

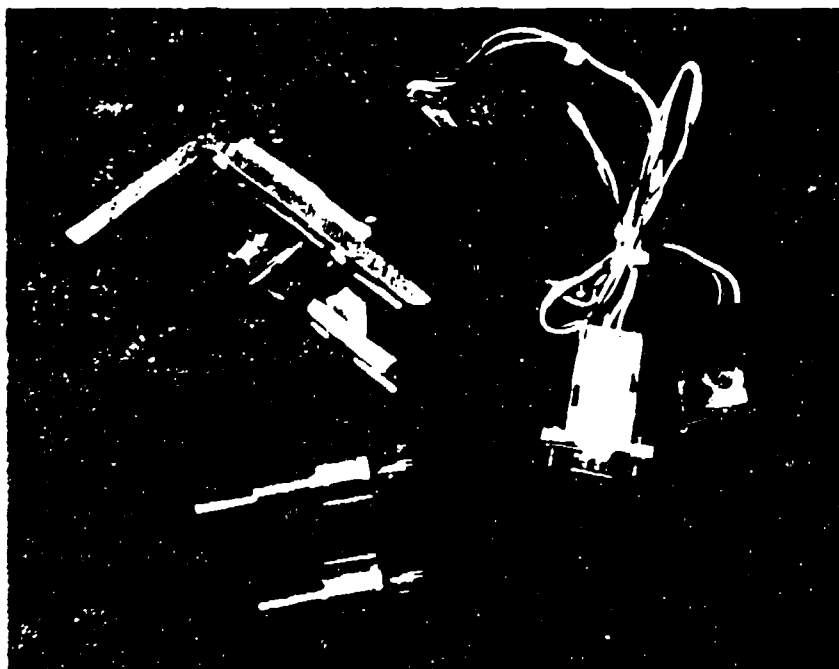
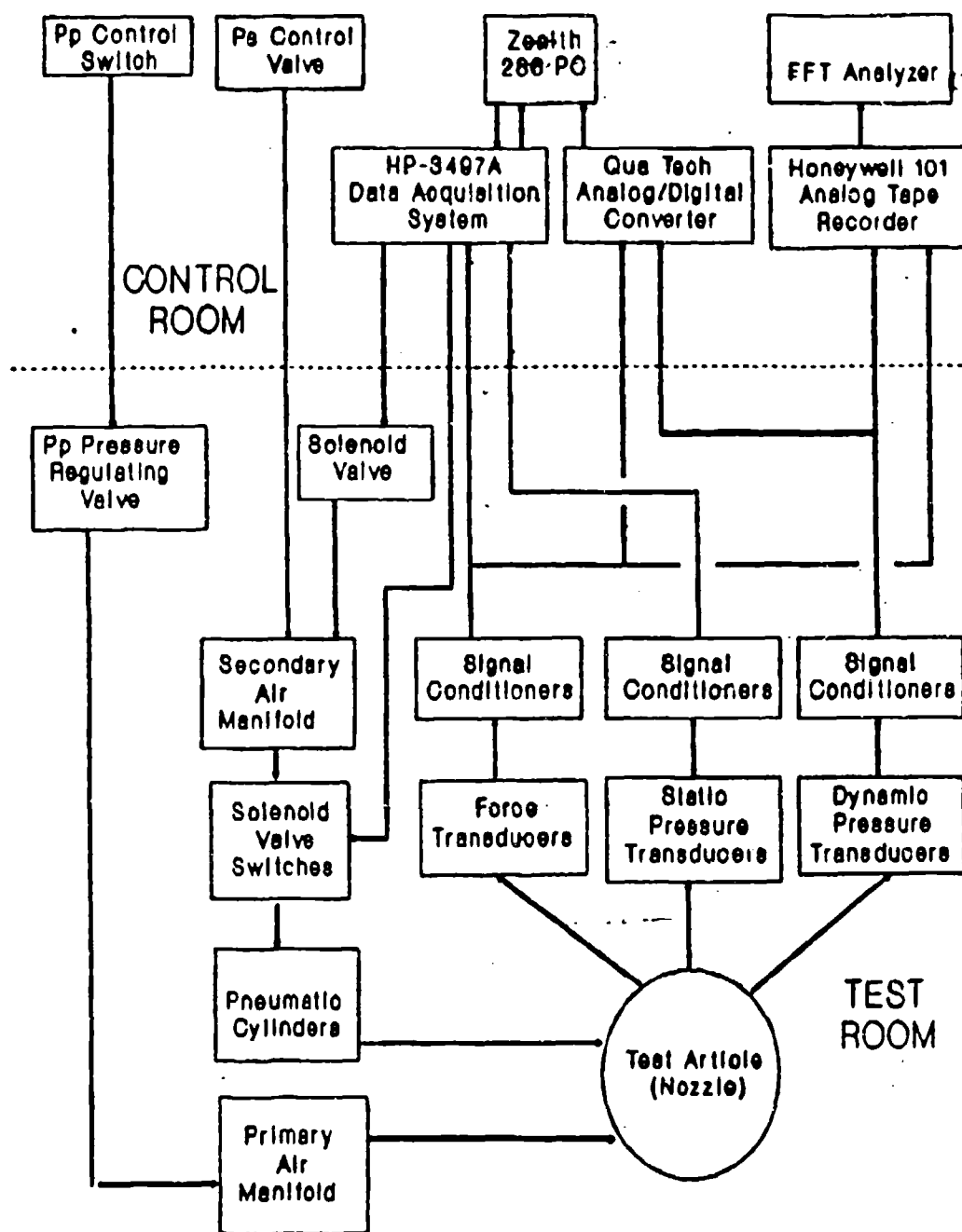


FIGURE 10 AIRFOIL ORIENTATION ASSEMBLY

D. Test Control and Instrumentation

All tests were conducted from the control room located behind the test stand. The control room provided protection from possible equipment failure and abated some of the nozzle noise. Hearing protection in the control room was required for test runs with primary pressures above 250 psig. All test operations; establishing primary and secondary pressures, vectoring commands, and data collection were commanded from the control room. Figure 11 presents a schematic of the test control and instrumentation system.

The instrumentation and control capability was significantly improved with the addition of a Zenith 286 personal computer (Z-286). The computer was connected to a Hewlett Packard 3497A (HP-3497A) data acquisition system. This enabled the solenoid valves and DC stepper motors to be commanded from the Z-286 keyboard in the control room. Survey data of "steady-state" axial and vectored test runs collected by the HP-3497A were processed by the Z-286 directly into ASCII files. The addition of a Qua Tech analog to digital converter board (A/D board) to the Z-286 enabled collection and storage of 4 channels of time tagged digital data directly into ASCII files. Using a quick BASIC computer program the A/D board was able to collect up to 2100 data points at a sample rate of 200 to 32,000 Hz (6). The control and data acquisition requirements were defined and two quick BASIC



**FIGURE 11 TEST CONTROL
/INSTRUMENTATION SCHEMATIC**

programs written to collect digital data and perform the probe insertion and airfoil orientation.

The Honeywell 101 analog tape recorder and the Hewlett Packard Fast Fourier Transform Analyzer enabled time domain analysis of the force balance and confined jet cylinder pressure transducer measurements. The highest frequency response of this recorder is 47 kHz at a tape speed of 120 kHz at a tape speed of 120 in/sec. All time domain data was recorded at 120 in/sec with the nozzle at steady state in axial or vectored operation (3).

1. Force Balance Axial and side forces were measured using the force balance shown in Figure 12. This force balance used two force transducers mounted on pivots so that each transducer was isolated from the other. The force transducers were strain gauge type transducers with a nominal range of +/-100 lbf and the voltage response was linear for forces up to +/-130 lbf. The forces encountered at the nozzle operating conditions of this study were within the linear range of the force transducers. The pivots allowed each transducer to be put into tension or compression without any lateral or shear forces. This enabled the net force in the plane of the floor to be resolved into axial and lateral forces. Any forces out of the plane of the force balance resulted in coupling between the two transducers. Flow visualization with a tufted grid at the nozzle exit was used

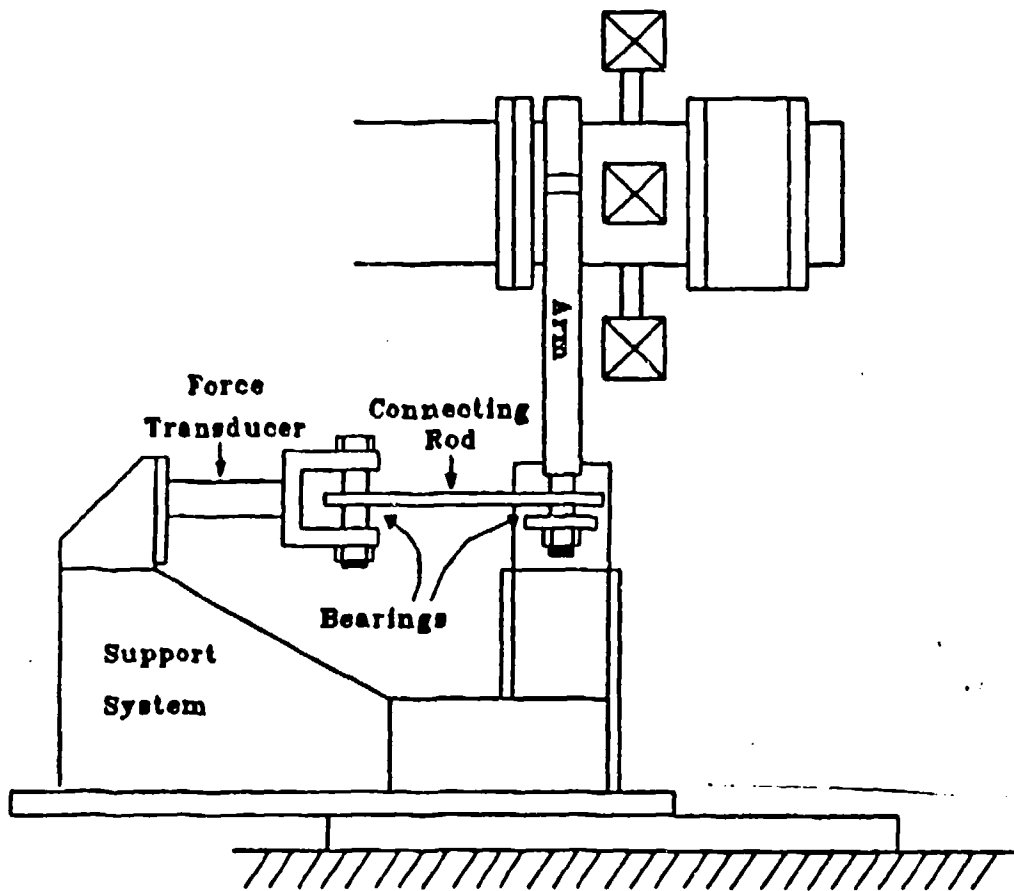


FIGURE 12 FORCE BALANCE

to insure that the nozzle configuration tested was either axial or vectored within the plane of the force balance. The force balance was found to have resonant frequencies at low frequencies when installed on the test stand. The amplitude of these low frequency oscillations was amplified significantly during vectored nozzle operation. These low frequency oscillations dominated the transient force response measurements and made evaluation of the force transient difficult.

2. Pressure Measurements Static wall pressures (P_w) were measured at axial locations (downstream of the insertion ports) within the nozzle using static pressure taps connected to ten Statham diaphragm pressure transducers with tygon tubing. Dynamic pressure fluctuations within the confined jet cylinder were recorded using two Endevco piezoelectric transducers: one in the plane of the probe thrust vector control disturbance and one out of the plane. All the transducers were calibrated in place with the instrumentation system using a static dead weight pressure calibrator. Thus, the calibration was accomplished for the entire data acquisition system using the voltages measured by the instrumentation system.

The operating pressures for each test run were set using the uncalibrated gauges in the control room. Pressure gauges mounted on the plenum and the secondary air manifold

were used to measure the operating conditions for the nozzle for data analysis. Tests are run at four stagnation pressures: 150, 250, 350 and 450 psig. The nominal values were set by hand in the control room and evaluated at the P_p value measured by the calibrated pressure transducers.

3. Data Processing Signals from all the transducers were transmitted through shielded cables to either the HP-3479A or the Qua Tech analog to digital converter. These voltage signals were in turn sent to the Z-286 and converted, using the transducer calibration data, into pressures and forces then stored in ASCII files. The data acquisition flow is shown in Figure 11. The ASCII data was then processed using Lotus 1-2-3 spreadsheets and graphed using the Lotus graphics package.

The time domain analysis of the force balance and cylinder pressure measurements was accomplished using the Honeywell 101 analog tape recorder and the HP-FFT analyzer. Steady state data was collected for the confined jet nozzle configuration in axial operation and vectored operation at various primary pressures. Fifteen frequency distribution 'snapshots' were averaged at each operating condition to resolve the dominant frequencies present during the nozzle operation.

III. Experimental Procedure

A. General

All electrical equipment was turned on and the signal conditioners were allowed to warm up for one hour prior to the beginning of test runs to allow the voltage levels to stabilize. The primary and secondary manual air valves in the test room were opened to charge the air supply system. The first stage primary air control valve was then primed from the control room using the 'load' switch on the control panel. At the start of a given test run the primary air was turned on and allowed to run until the plenum air stagnation temperature stabilized. For any test run the primary and secondary air pressures were set using the second stage primary air control valve 'load' switch and the manual secondary air valve on the control panel. Once the plenum air pressure stabilized at the set value, in either axial or vectored nozzle operation, data acquisition was initiated. Following data acquisition the plenum pressure was set to the next value and the data acquisition process repeated. At the completion of a test series the second stage primary air valve was vented using the 'vent' switch on the control panel. The secondary air manifold was vented by opening a solenoid valve with a command from the HP-3497A. All test series were

repeated to ensure that the test procedure yielded consistent results.

B. Data Acquisition

The data acquisition process was greatly facilitated with the use of two quick BASIC programs. This enabled the cylinder insertion/extraction and airfoil orientation devices to be commanded remotely from the Z-286. The analog transducer signals were digitized and loaded directly into ASCII files.

The first program was the 'workhorse' throughout this study. Several control and data acquisition subroutines were tied to the function keys on the Z-286 keyboard. The 'zero run' took readings of the transducer voltages by the HP-3497A, storing them into an array as a DC offset voltage. Each transducer was read eleven times and an average value stored into the DC offset array. This provided repeatable measurements within the transducer error. The 'zero run' subroutine was used in conjunction with the 'static run' subroutine. The 'static run' subroutine was essentially the same as the 'zero run' subroutine except that the force balance transducers were read fifty times and averaged due to the oscillation of the 'steady state' readings. This provided repeatable measurements for the force balance transducers to ± 0.50 lbf. The DC offset voltages from the 'zero run' subroutine were subtracted from the voltages collected during

the 'static run' subroutine. These voltages were then converted to pressures and forces using the transducer calibration data and stored into an ASCII data file.

Two other function keys ran subroutines called: 'dynamic run insertion' and 'dynamic run extraction'. These subroutines configured the A/D board for the sample rate and number of data points for a given insertion/extraction. This dictated the time 'snapshot' of data recorded based on the equation: $\text{time duration} = (\text{number of data points}) / (\text{sample rate})$.

From the software checkout it was found that the insertion command took approximately 10-20 ms to reach the pneumatic cylinder through the HP-3497A/solenoid valve control chain. The extraction command required 60-80 ms on average. The delays associated with the insertion and extraction commands ensured that the vector transient appeared in the middle of the data window. This provided data on the status of the nozzle before and after the vector command was given. Once the A/D board was configured the data could be acquired and converted to pressures and forces by the Z-286. This data was then stored into ASCII files for later data reduction.

The second program was the airfoil orientation program. The DC stepper motor controller was directly connected to the Z-286. The motors could then be commanded to rotate through a designated angle, direction, and at a

designated speed. Since the motors were mounted 180 degrees from each other it was necessary to reverse the polarity of one of the motors to enable both to rotate in the same direction. This was accomplished with a software command to the motor controller.

C. Steady State Axial Runs

These tests were performed to characterize the axial operation of the conical nozzle and confined jet nozzle. Axial thrust and the static pressure distribution within the nozzle were measured for plenum pressures ranging from 150-450 psig. A steady state or static test is where the probe is set to a given insertion depth, or angle of attack in the case of the airfoil probe, and the nozzle is brought to steady-state at the primary pressure of interest. The insertion depth for axial pin probe thrust vector control tests was zero. Tests were conducted using the 'static run' subroutine.

D. Steady State Vectored Runs

These tests evaluated the effect of the probe thrust vector control mechanisms using averaged force balance data. The nozzle was brought to steady state for a given probe thrust vector control configuration and plenum pressure. Data was then collected using the 'static run' subroutine.

E. Vector Transient Runs

Transient run data was acquired in two ways. Real time force and confined jet nozzle cylinder pressure data were obtained using the A/D board. This enabled evaluation of the vector time response. Due to the inherent ringing of the force balance the static pressure at the confined jet cylinder wall (psig) was found to be the most useful for evaluations of vector time response runs. The static pressure at the confined jet cylinder wall measurement was only possible on the confined jet nozzle configuration as there was no provision to mount dynamic pressure transducers in the conical nozzle.

Frequency evaluations were performed using the Honeywell 101 and the HP-FFT analyzer. These tests were performed to evaluate the frequency response of the force and pressure transducers during steady state axial and vectored operation of the nozzles. During these tests, the nozzle was brought to steady state in either axial or vectored operation before data was recorded on the Honeywell 101. Once a series of tests were completed for a given configuration the data was played back through the signal analyzer. Using the FFT function fifteen data snapshots were averaged in the frequency domain to evaluate dominant frequencies. Fifteen snapshots were found to provide repeatable frequency spectrums for the force transducers.

IV. Test Results and Discussion

A. Axial Operation

The conical nozzle and confined jet nozzle were run "clean," where clean indicates that the probe thrust vector control devices were backed completely out of the flow. The insertion ports were sealed with the static cylindrical pins inserted to zero pin insertion depth. This configuration left a small depression at the injection port along the nozzle wall. Although this was not a smooth wall, stable axial flow was possible for both the conical nozzle and confined jet nozzle at P_p 's higher than 130 psig. Stable axial flow is where the lateral force fluctuation is nominal (± 0.5 lbf) around a steady state value of zero.

The static pressure at the static pressure tap locations along the wall of the nozzle (P_w) were surveyed for both the confined jet nozzle and conical nozzle for P_p 's ranging from 150-470 psia at approximately 50 psia increments. These P_w surveys give a good indication of the flow condition within the diverging nozzle section for both configurations. These surveys are presented in Figures 13-16 in two ways for both configurations: P_w vs P_p and P_w vs L_a . L_a indicates the axial location of the static pressure tap measured from the downstream edge of the nozzle throat. The lines in each figure indicate a family of data points and not actual

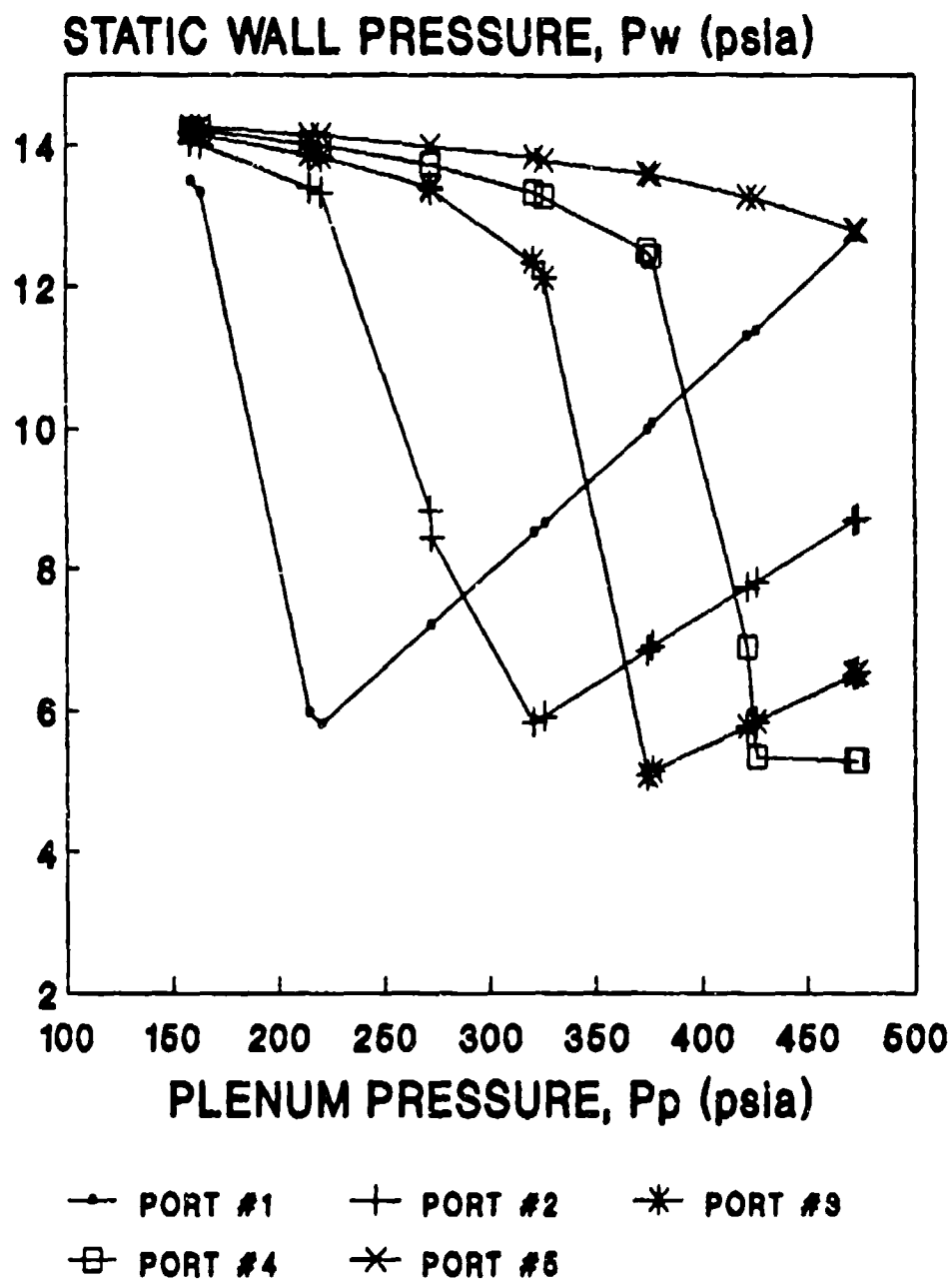
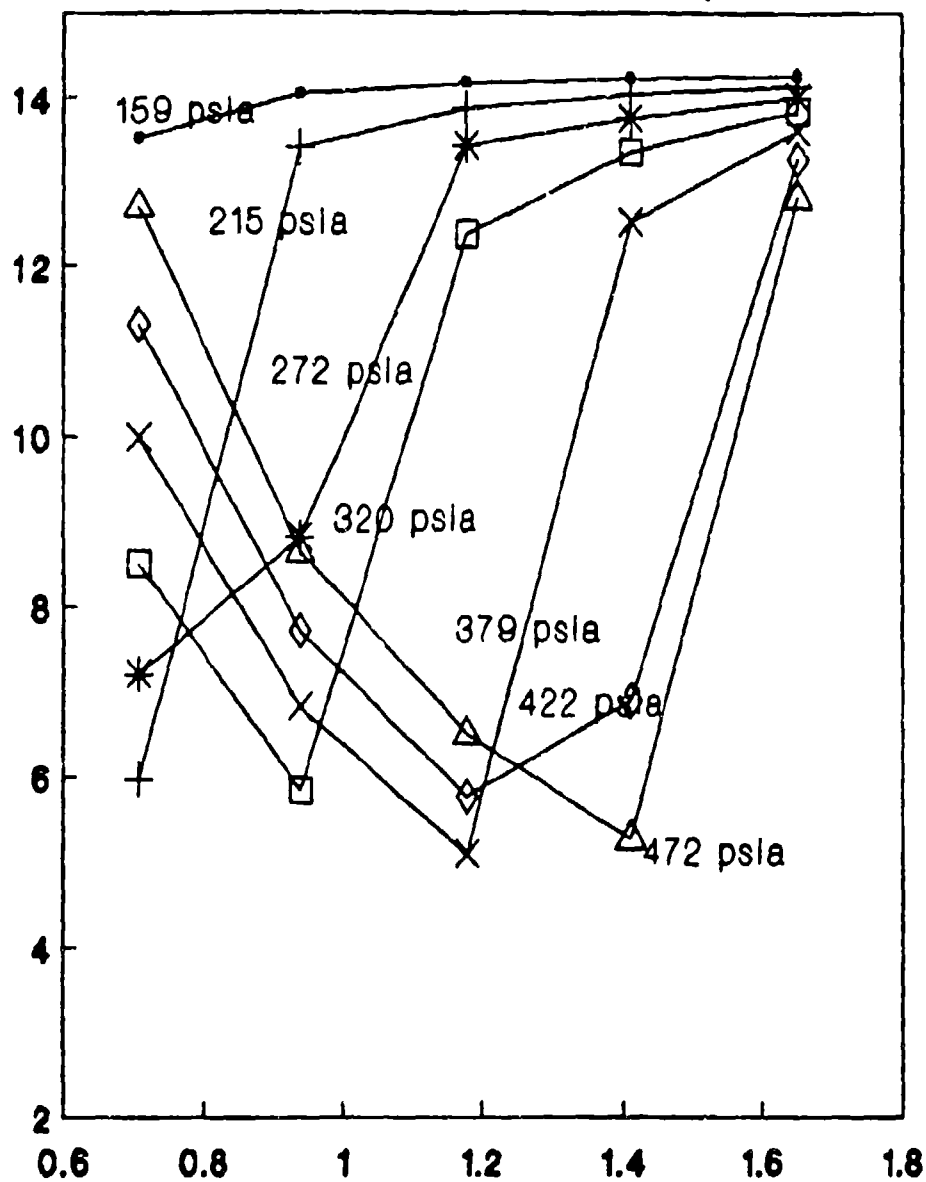


Figure 13. Conical Nozzle Flow Condition at Static Pressure Tap Locations

STATIC WALL PRESSURE, P_w (psia)



AXIAL DISTANCE FROM THROAT, L_a (in)

Figure 14. Conical Nozzle Flow Condition at Static Pressure Tap Locations for Various Plenum Pressures

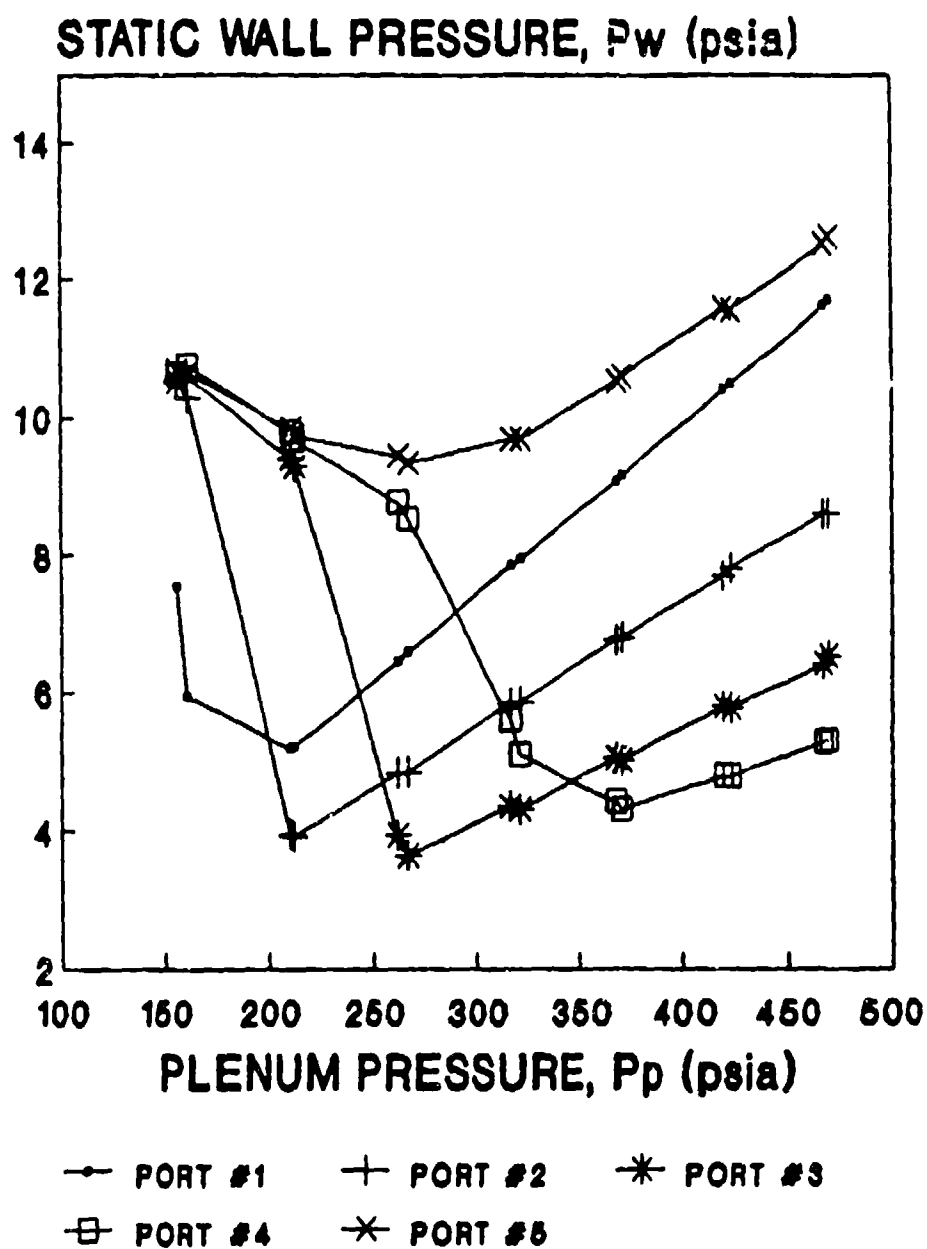


Figure 15. Confined Jet Flow Condition at Static Pressure Tap Locations

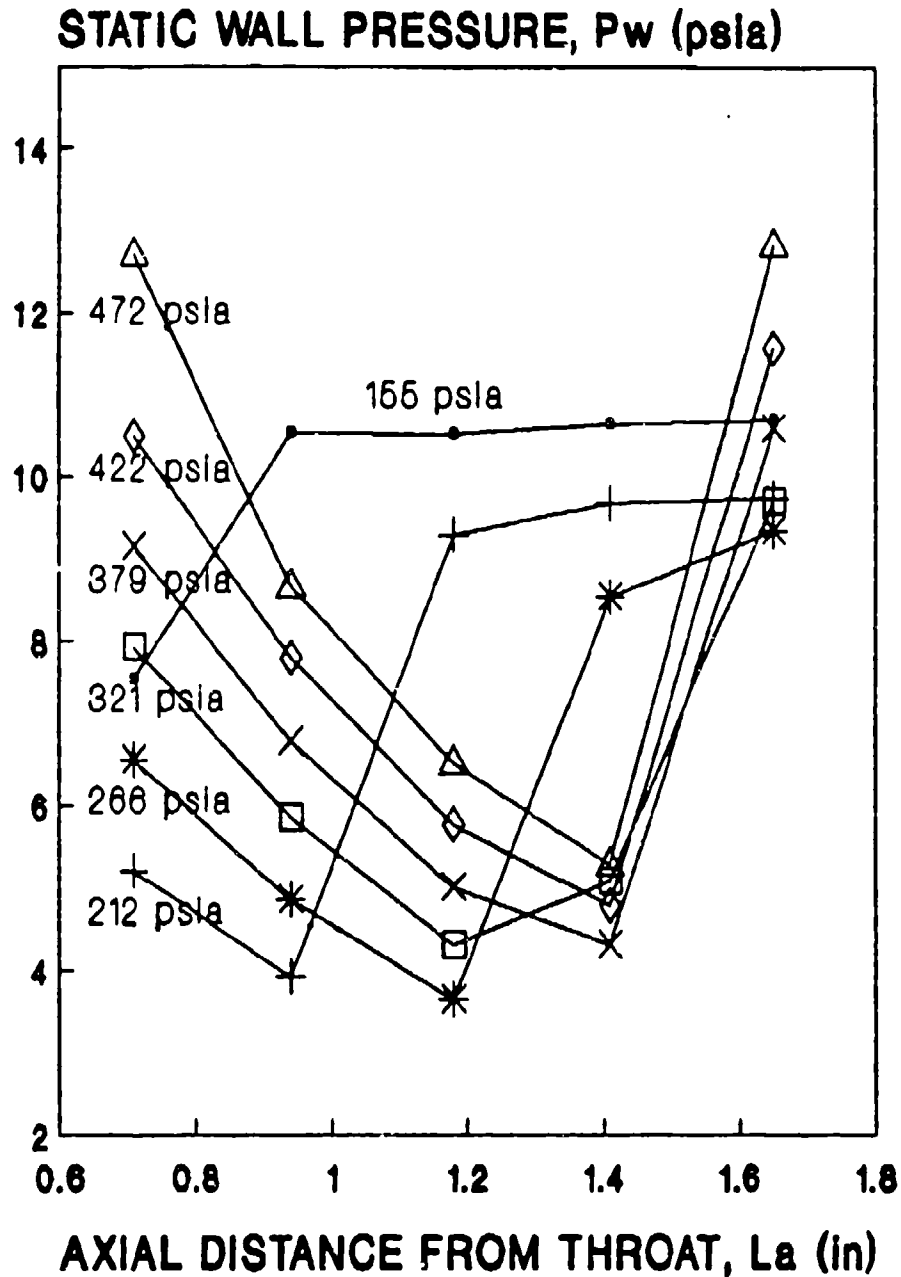


Figure 16. Confined Jet Flow Condition at Static Pressure Tap Locations for Various Plenum Pressures

pressure variation. Figures 13 and 15 show P_w vs P_p and show how the flow condition changes at each static pressure tap as P_p varies for the conical nozzle and confined jet nozzle. The point where the flow is overexpanded and separates from the nozzle wall can be seen where P_w begins to increase linearly as predicted by the isentropic nozzle equations (3). Figures 14 and 16 show how the separation point moves downstream from the nozzle with increasing P_p . Figure 17 is included to show the area ratio of the conical nozzle ($AR_{cn} = A_a/A_t$) along the diverging section at each static pressure tap location and the area ratio of the confined jet ($AR_{cj} = A_a/A_{ec}$). It should be noted that the AR_{cn} is the same for the confined jet nozzle in the diverging section. In the case of the confined jet nozzle AR_{cj} can be more informative in locating the separation point as will be discussed later.

Figures 13-16 indicate that for increasing P_p a separation point moves downstream from the nozzle throat for both configurations. During axial operation the nozzle core flow expands at supersonic velocity until the given local static pressure cannot support this expansion. The flow then separates from the nozzle wall creating a core nozzle flow and a separation region along the remainder of the nozzle wall. The separation point is defined as the point where P_w begins to increase linearly as predicted by the isentropic nozzle equation. In Figures 13 and 15 the separation point can be

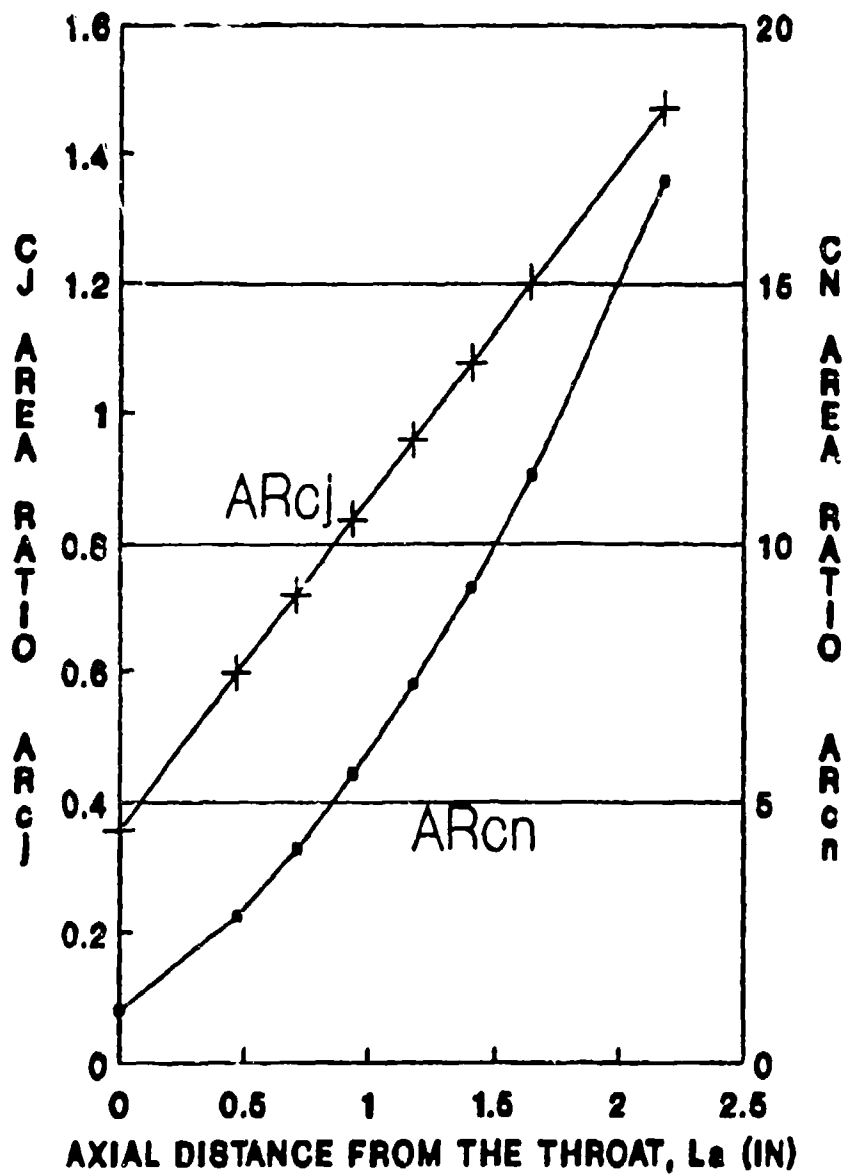


Figure 17. Area Ratio for CN (AR_{cn}) and CJ (AR_{cj}) for Axial Locations in the Nozzle Section

located approximately at or slightly upstream from where P_w begins to increase linearly with P_p .

Figures 13 and 14 present an overview of the flow condition of the conical nozzle during axial operation for various plenum stagnation pressures (P_p). Both figures show that the conical nozzle is overexpanded at all the pressure taps for P_p around 150 psia. As P_p increases to 215 psia, the static wall pressure drops significantly indicating that the normal shock associated with flow separation has moved past the first static tap location. The axial location of the separation point in the conical nozzle can be located generally from Figure 14 and is summarized in Table 3.

Table 3
Axial Location of Separation Point (L_s) in Conical Nozzle

<u>P_p (psia)</u>	<u>L_s</u>
159	Upstream of Port #1
215	Port #1 < L_s < Port #2
272	Port #1 < L_s < Port #2
320	Port #2 < L_s < Port #3
379	Port #3 < L_s < Port #4
422	Port #3 < L_s < Port #4
472	Port #3 < L_s < Port #4

Figures 15 and 16 present an overview of the flow condition of the confined jet nozzle during axial operation. It is apparent from Figure 15 that the separation point is near Port #1 at P_p 155 psia. This is indicated by the significant drop in static wall pressure from the conical nozzle in Figure 13. This indicates that the flow for the

confined jet nozzle is fully expanded and supersonic at the insertion port. The axial location of the separation point in the confined jet nozzle can be located generally from Figure 16 and is summarized in Table 4.

Table 4
Axial Location of Separation Point (Ls) in Confined Jet Nozzle

<u>Ep (psia)</u>	<u>Ls</u>
155	Upstream of Port #1
212	Port #1 < Ls < Port #2
266	Port #2 < Ls < Port #3
321	Port #3 < Ls < Port #4
379	Port #3 < Ls < Port #4
422	Port #3 < Ls < Port #4
472	Port #3 < Ls < Port #4

The separation point in the diverging nozzle is further downstream of the nozzle throat for the confined jet nozzle than the conical nozzle for a given plenum supply pressure. This is due primarily to the pressure ratio across the diverging nozzle itself. The conical nozzle exhausts to ambient pressure. The confined jet nozzle has an artificial ambient pressure that is lower than the true ambient pressure. This can be seen clearly from Figure 14 and 16 where the downstream pressure is near atmospheric for the conical nozzle and significantly lower for the confined jet nozzle. The larger pressure ratio across the nozzle allow the confined jet nozzle flow to remain attached further downstream than for the conical nozzle.

Figures 15 and 16 indicate an interesting operating characteristic of the confined jet nozzle configuration. The separation point of a confined jet depends on two primary factors: P_p and A_{ec} . As P_p is increased, the separation point moves downstream until it reaches a quasi equilibrium point. This equilibrium point is determined when the core flow seals the confined jet nozzle cylinder section from the ambient pressure. The confined jet nozzle cylinder pressure then begins to rise with increasing P_p tending to stabilize the separation point.

Friddell (3) found that the stabilization point occurred where the area of the nozzle at the separation point (A_s) is approximately equal to the end cap exit area (A_{ec}) or $A_s/A_e = 1.0$. It can be seen from Figures 15 and 16 that the separation point for this confined jet nozzle tends to stabilize around 1.2 in $< L_a < 1.4$ in at $P_p > 370$ psia. This result is close to Friddell's data where he postulated the separation point for the same nozzle as $L_a = 1.18$ in. Figure 17 indicates that $A_{ec}/A_t = 1.0$ at $L_a = 1.25$ in. This is in the region where the separation point stabilized during axial test with the confined jet nozzle.

Figure 18 presents the non-dimensional axial force (NDFa) vs. P_p characteristics of three configurations: conical nozzle, confined jet nozzle, and the conical nozzle with the

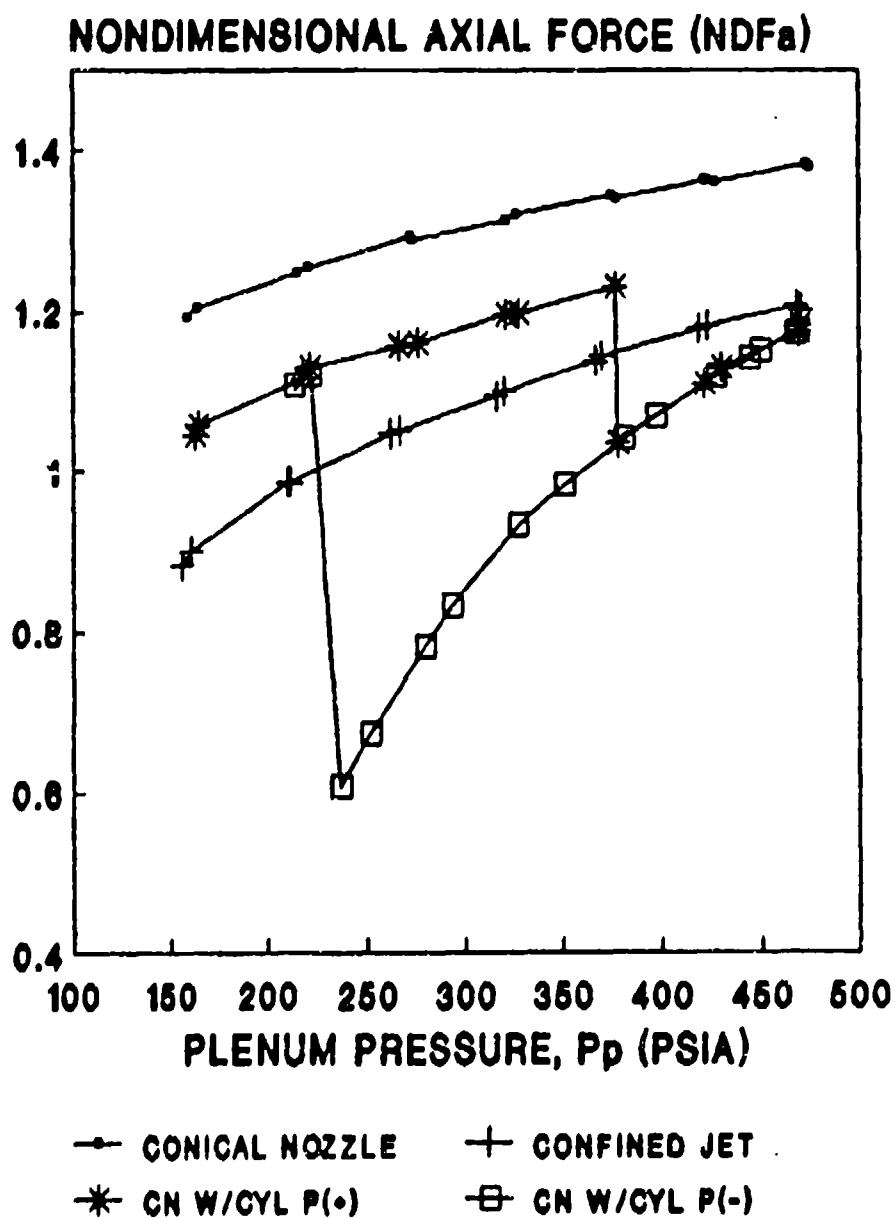


Figure 18. Nondimensional Axial Force Vs Plenum Pressure for Various Test Configurations

confined jet nozzle cylinder attachment without end cap. The Nondimensional Axial Force, $F_a/P(P_p A_t)$, was computed by dividing the measured axial force (F_a) by P_p and A_t . This provides a crude measure of thrust coefficient. The difference between the conical nozzle and confined jet nozzle curves indicates the thrust penalty associated with using the confined jet nozzle. The data for the confined jet nozzle compare closely with the baseline axial data for the same nozzle by Herup (4) and Friddell (3). The penalty is largest at low P_p , approximately 25%, and decreases to around 10% at high P_p .

The conical nozzle with cylinder configuration was tested by increasing and decreasing P_p through the entire P_p range. It was found that during increasing P_p tests the flow would expand along a force curve between the conical nozzle and confined jet nozzle curves as shown in Figure 18. It would continue along this curve until the core flow would attach to the confined jet nozzle cylinder section. This result corroborates that of by Friddell (3). At attachment, the nondimensional axial force, $F_a/(P_p A_t)$, would drop significantly below the confined jet nozzle curve and begin to asymptotically approach it from below. However, it was found that by decreasing the P_p from the maximum the flow would remain attached to the confined jet nozzle cylinder well past $P_p = 380$ psia where the flow attached at increasing P_p .

The flow remained attached until it reached $P_p = 245$ psia where it returned to the P_p increasing curve. This is an interesting result from a design standpoint. If a device were used to convert an operating conical nozzle to a confined jet this phenomenon could be of interest. It is assumed that the points of attachment and detachment depend primarily on pressure ratio and cylinder length. Longer cylinder lengths would impinge on the expanding free jet causing attachment at lower pressure ratios.

B. Vectored Operation

During this portion of the investigation the cylindrical pins and double wedge airfoils were evaluated as probe thrust vector control devices in the conical nozzle and confined jet nozzle configurations. These tests were performed with the nozzle in a steady vectored state at various P_p 's and pin insertion depth's.

Cylindrical Pins in the Conical Nozzle. The pin insertion depth's tested in this configuration represented various percentages of the distance from the insertion port at the nozzle wall to the nozzle centerline (0%-96%). Figure 19 shows the changes in nondimensional axial force, $F_a/(P_p A_t)$, with changes in P_p for several pin insertion depth values for the conical nozzle using one pin at the insertion port ($L_a = 0.47$ in). Figure 19 shows a significant drop in the vectored nondimensional axial force, $F_a/(P_p A_t)$ values from the axial

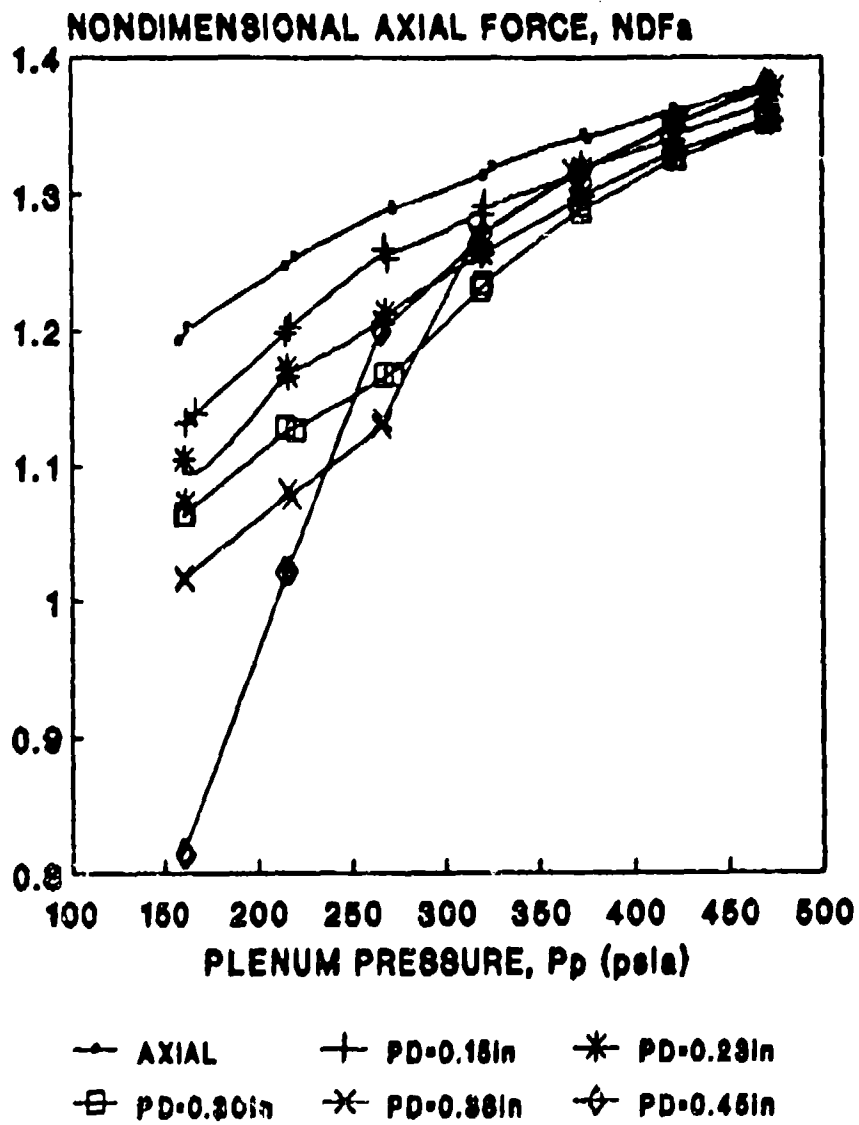
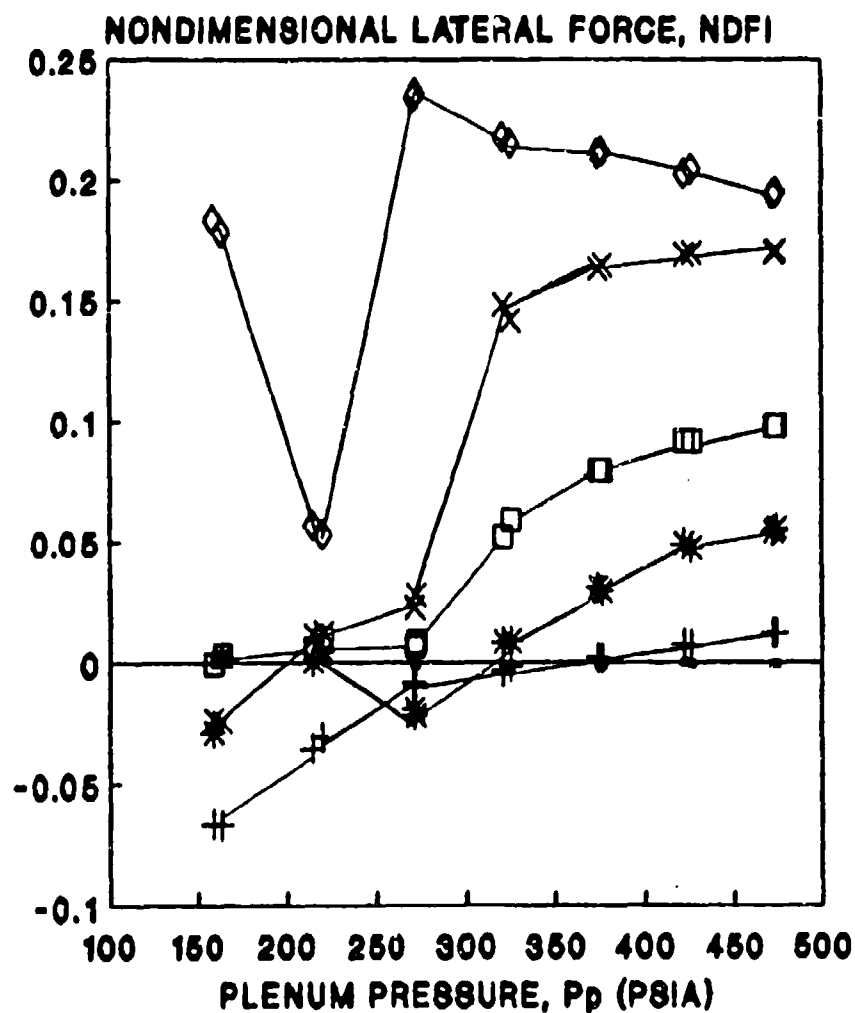


Figure 19. Conical Nozzle NDFa vs P_p for Various PDs

nondimensional axial force, $F_a/(P_p A_t)$ values at low P_p . As P_p is increased above 260 psia the vectored values begin to asymptotically approach the axial nondimensional axial force, $F_a/(P_p A_t)$, values. Figures 13 and 14 indicate that the separation point for the conical nozzle occurs just downstream of the insertion port at plenum stagnation pressures less than 260 psia. This indicates that as the normal shock increases in strength, the flow losses relative to the axial thrust decrease. The bow shock created by the pin disturbance at low P_p is not strong enough to overcome the impingement or blockage of the pin (especially at the larger pin insertion depth's) on the vectored flow.

Figure 20 shows the vectored nondimensional lateral force, $(F_l/(P_p A_t))$, versus P_p for the conical nozzle. Nondimensional lateral force, $F_l/(P_p A_t)$ is calculated in the same manner as nondimensional axial force, $F_a/(P_p A_t)$, using F_l instead of F_a . This figure shows some interesting trends. First, at P_p 's above 300 psia the conical nozzle is fully expanded in axial operation well past the pin disturbance (see Figures 13 and 14). Figure 20 shows that the nozzle was vectored at all pin insertion depth's except $PD = 0.38$ inches in this pressure regime. The nondimensional lateral force, $(F_l/(P_p A_t))$, appears to approach a limiting value for each pin insertion depth tested. This result is similar in magnitude for $PD = 0.38$ in to the results obtained by Friddell (3) using



• AXIAL + PD=0.18in * PD=0.23in
 □ PD=0.30in × PD=0.38in ◇ PD=0.45in

Figure 20. Conical Nozzle NDFI vs P_p for Various PDs

secondary injection thrust vector control in the same nozzle. This data indicates that use of pins as a probe thrust vector control device in a fully expanded nozzle is viable with lateral forces up to 12% or more of the axial force.

Second, the data shows some interesting effects in the P_p range below 300 psia. This is where the axial separation point is in the proximity of the insertion port. This appears to be an unstable region for probe thrust vector control in the conical nozzle. Unstable here means that pin disturbance creates the unexpected result were the flow attaches to the nozzle wall with the pin disturbance. Figure 14 indicates this is a region where the separation point for axial flow occurs just downstream of the insertion port. A significant drop in nondimensional lateral force, $F_l/(P_p A_t)$, is seen at P_p around 200 psia. This is where the axial separation point occurs at the insertion port. At P_p 's slightly higher and lower than 200 psia the nozzle flow appears to attach to the side of the nozzle with the pin disturbance for pin insertion depth's less than 0.30 in. Flow attachment to the pin is designated as a negative lateral force, or a lateral force in the direction of the pin. Using larger pin insertion depth's at plenum pressure below 300 psia the flow vectoring is minimal, with the exception of pin insertion depth = 0.45 in where the flow is fully vectored. Figure 21 shows a ratio of nondimensional lateral force, $F_l/(P_p A_t)$ /nondimensional axial

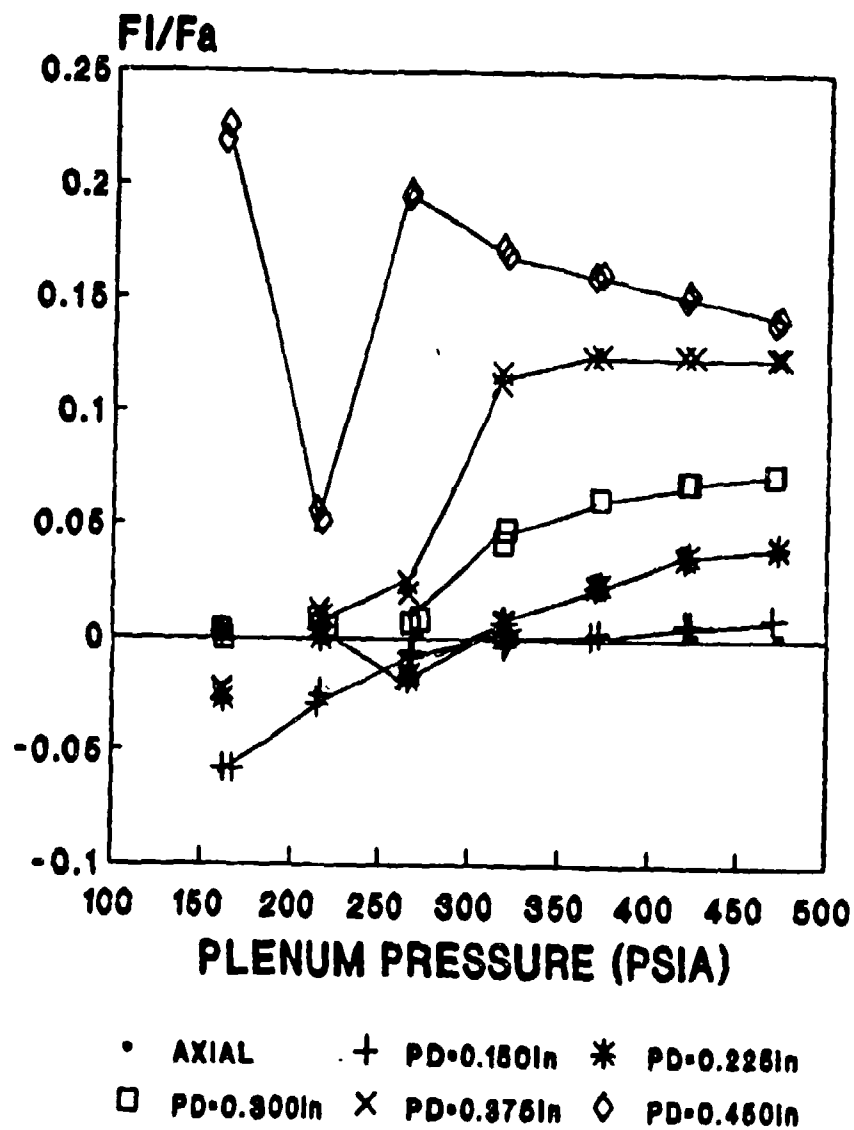


Figure 21. Conical Nozzle Force Ratio (F_I/F_a) vs P_p for Various PDs

force, $F_a/(P_p A_t)$, versus P_p . This figure shows the same trends as Figure 20, where the vectored lateral force is presented as a percentage of the vectored axial force.

Cylindrical Pins in the Confined Jet Nozzle. Unlike the conical nozzle, the confined jet nozzle was more responsive to probe thrust vector control pin disturbances. Figure 22 shows the nondimensional axial force (NDFa) vs plenum pressure (P_p) for the confined jet at various pin insertion depths. The confined jet nozzle was found by Herup (4) to vector in static insertion tests at pin insertion depth's ranging from 0.08 in to 0.20 in. The data shows that the nondimensional axial force, $F_a/(P_p A_t)$, reduction associated with pin probe thrust vector control at all pin insertion depth's was about the same regardless of pin insertion depth. The confined jet nozzle nondimensional axial force, $F_a/(P_p A_t)$, values follow the same curve as the axial NDFa values shifted down due to deflection of the nozzle flow. The vectored NDFa ranged from 75% of the axial value at low values of P_p to 85% at high values of P_p . If there is a trend for NDFa versus pin insertion depth the resolution of the force balance measurement was unable to resolve it. It appears that once the flow is disturbed into a vectored condition the axial nondimensional axial force, $F_a/(P_p A_t)$, produced is fairly independent of pin insertion depth.

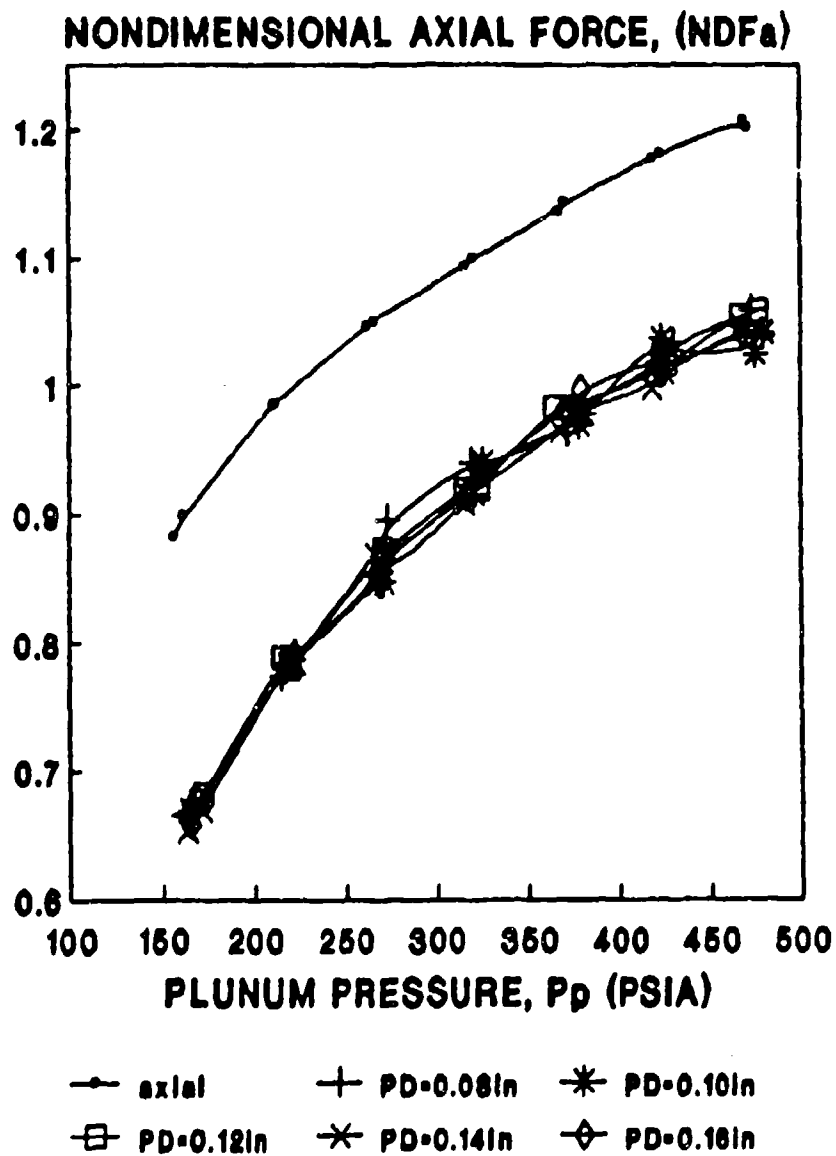
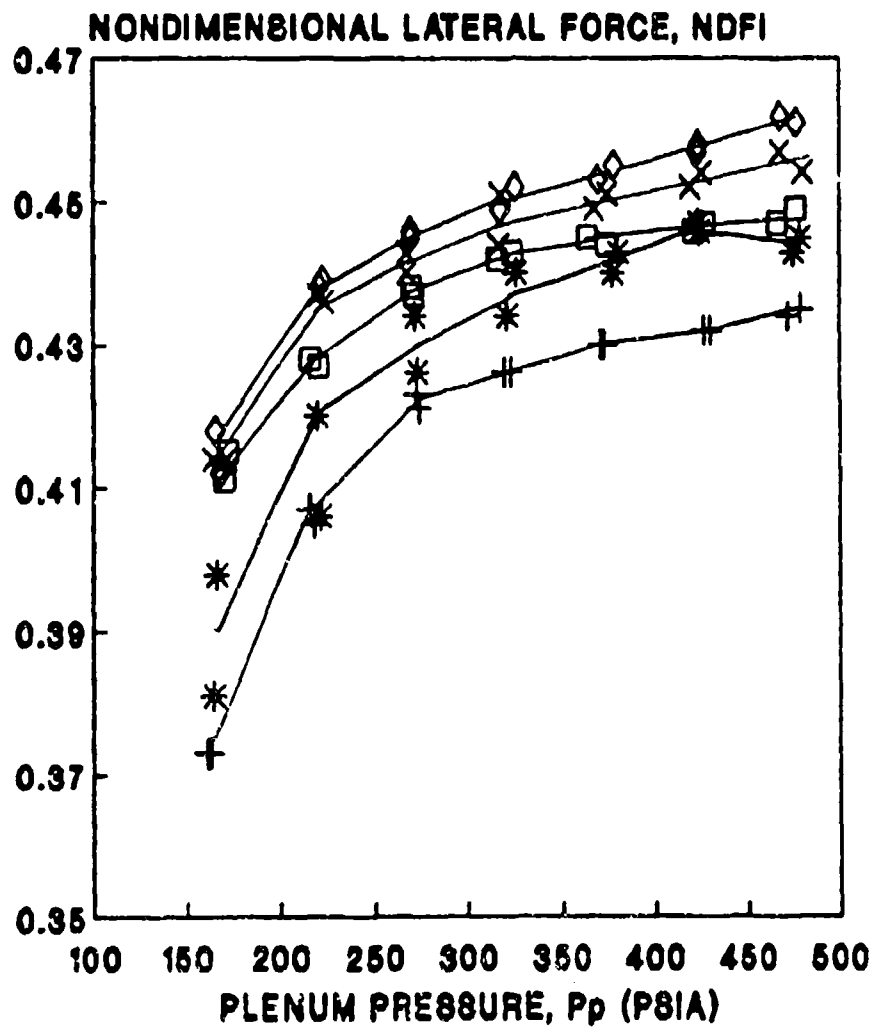


Figure 22. Confined Jet NDF_a vs P_p for Various PDs

Figures 15 and 16 indicate the separation point for the confined jet nozzle is downstream of the insertion port at the lowest P_p value (150 psia). This indicates that in an axial confined jet nozzle the flow is fully expanding and supersonic at the insertion port throughout the P_p range of this study. Since the flow is supersonic at the pin disturbance the bow shock is stronger due to the higher local Mach number than for the conical nozzle. In addition, once the flow is disturbed into a vectored condition the confined jet nozzle has more surface area for the flow to attach to in the confined jet nozzle attachment than the conical nozzle.

Figure 23 shows the nondimensional lateral force (NDF1), versus P_p for various pin insertion depth's. This figure shows a definite trend of nondimensional lateral force, $F_l/(P_p A_t)$, versus pin insertion depth. The smaller pin insertion depth's produce smaller lateral forces. As pin insertion depth is increased the lateral force increases toward a limiting value for each pin depth curve. This result compares with Herup (4:46) where he found that the NDF1 produced by the confined jet nozzle approached a limiting value of 0.5 using secondary injection. Although this trend is observable, the difference between the nondimensional lateral force values for the maximum and minimum values of pin insertion depth is approximately 10%. The variation of the nondimensional lateral force, $F_l/(P_p A_t)$, values for a given



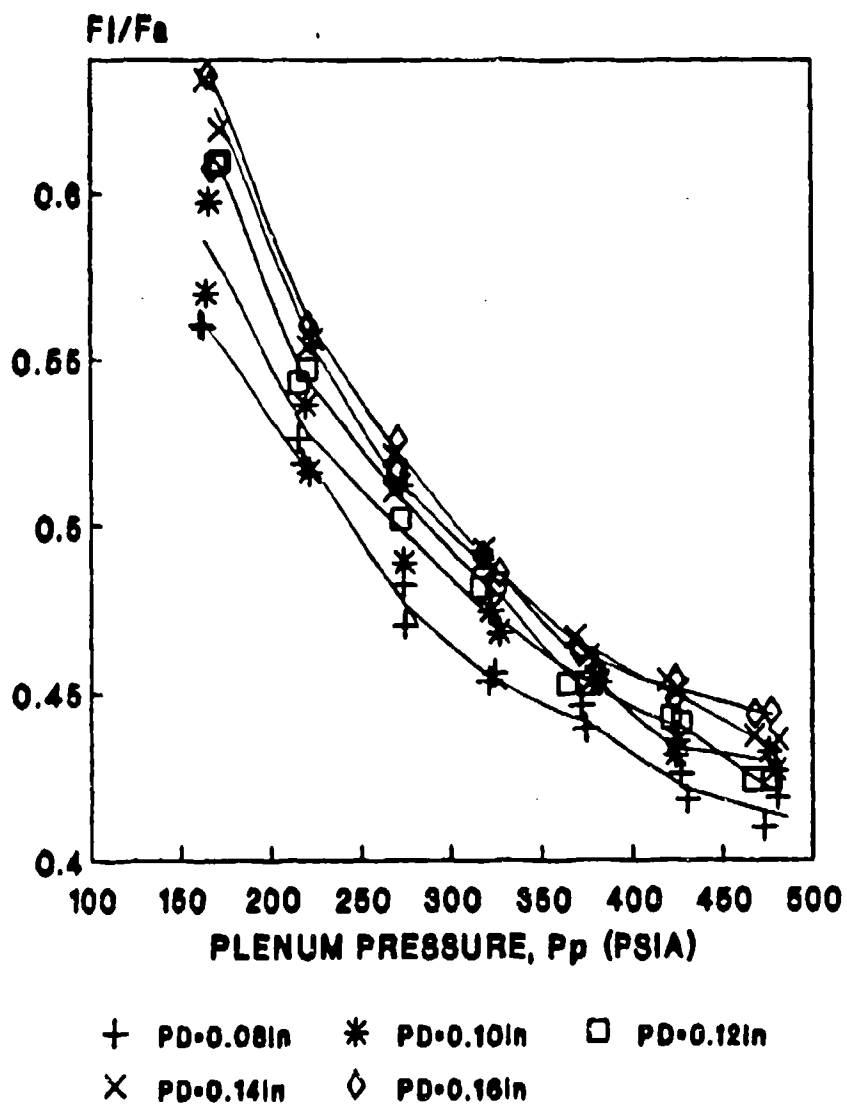
+ PD=0.08in * PD=0.10in □ PD=0.12in
 X PD=0.14in ◇ PD=0.16in

Figure 23. Confined Jet NDFI vs. P_p for Various PDs

pin insertion depth curve is due to the uncertainty involved in setting the pin insertion depth's with the threads on the set pins.

Figure 24 shows the ratio of F_l/F_a versus P_p . This figure shows the same trend as Figure 23 in that large pin insertion depth's produce larger lateral forces. The F_l/F_a ratio decreases from an average of 0.6 at low P_p to an average of 0.43 at high P_p . This is due to the percentage increase in F_l being smaller than the corresponding increase in F_a as P_p increases.

Double Wedge Airfoils (DWA) as a probe thrust vector control Device Herup (4) found that the confined jet nozzle could be vectored using airfoils rotated at an angle of attack relative to the nozzle centerline. During these tests four airfoils were inserted into the air flow to a given airfoil insertion depth. Airfoil insertion depth is defined in the same manner as pin insertion depth. He found in static tests that axial flow was possible with the confined jet nozzle with the airfoils set at zero angle of attack and that flow could be vectored out of the plane of the probe thrust vector control disturbance by rotating the airfoils to 45 degree angle of attack. He postulated that it might be possible to control the orientation of the lateral force by rotating the airfoils. These results could not be repeated during this investigation. It was found during this



**Figure 24. Confined Jet Force Ratio (F_1/F_a)
vs P_p for various PDs**

investigation that the nozzles were very sensitive to airfoil insertion depth. Using the rotating airfoil assemblies airfoil insertion depth was set within 0.01 in using a feeler gauge and the airfoils rotated to zero angle of attack. During tests the conical nozzle and confined jet nozzle would vector immediately upon startup away from the inserted airfoil that created the largest disturbance. The conical nozzle and confined jet nozzle could be made to vector using a single airfoil inserted and rotated to 90 degrees angle of attack. With the airfoil rotated at 90 degrees it presented the same disturbance to the airflow as a pin inserted to the same distance with the same results. The sensitivity of the nozzle to airfoil insertion depth limits the utility of the rotating airfoils as a probe thrust vector control device.

C. Vector Time Response Data

The evaluation of the vector time response depended primarily on the instrumentation response time. The force balance time response dominated the force time response data. The confined jet nozzle cylinder pressure provided a reasonable measurement of the nozzle response.

Force Balance Frequency Response The low resonant frequency of the force balance used in this investigation made real time force data virtually unusable for transient analysis. This was evaluated by subjecting the force balance to impulsive forces to evaluate the natural frequencies of the

axial and lateral transducers of the force balance. Figures 25 (axial) and 26 (lateral) show the frequency distribution of the force balance transducers to axial and lateral impulsive forces. The nozzle assembly was hit with a rubber mallet along each axis. FFT analysis using the HP-signal analyzer revealed that the axial transducer had a natural frequency around 40 Hz and the lateral transducer exhibited coupled frequencies at 55 Hz and 200 Hz to impulsive loads applied in the axial direction. Lateral tests revealed the lateral transducer natural frequency to be around 48 Hz with little coupling exhibited by the axial transducer. The consequences of this was exhibited by the oscillation in all the force balance data.

Axial tests revealed that the measured values in "steady state" operation of the confined jet nozzle revealed dominant frequency components for both transducers. The frequency components of the force measurements changed slightly with changes in P_p (or the loading on the force balance). In general the axial transducer exhibited dominant low frequencies at 43 Hz and 200 Hz. At $P_p = 150$ psia this frequency moved down to 38 Hz for P_p 's greater than or equal to 250 psia. The lateral transducer exhibited frequencies at 9, 55, 135, 200 Hz. The amplitude of these oscillations grew with increasing pressure. A representative frequency spectrum of the force balance response is presented as Figure 27. A

REAL-TIME AVG COMPLETE

Src

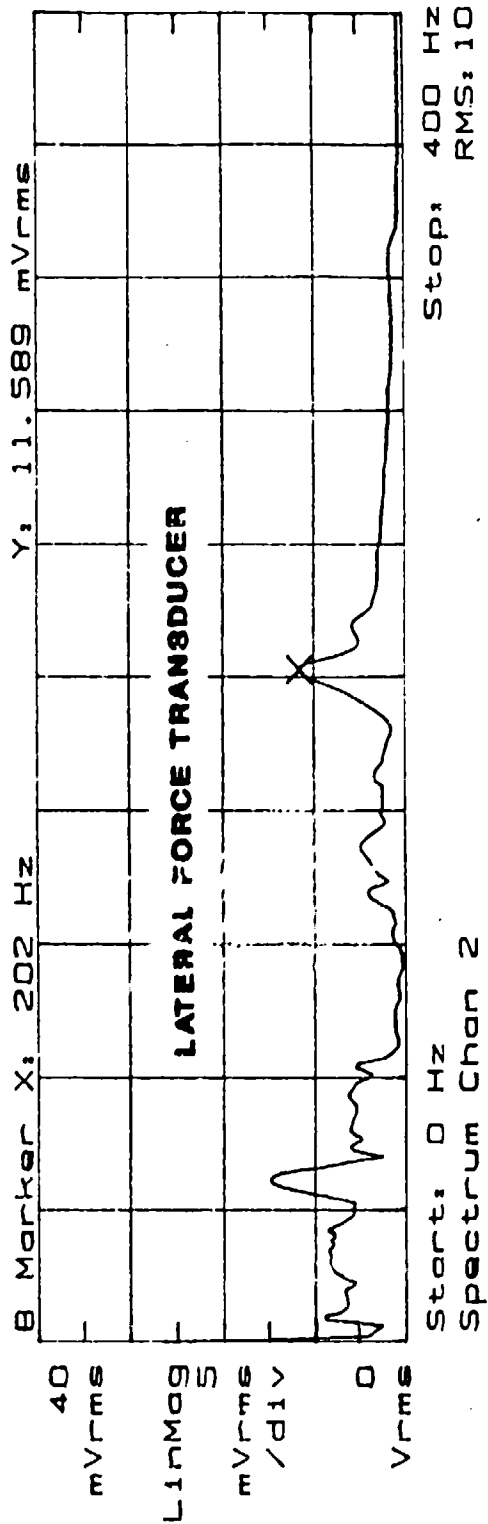
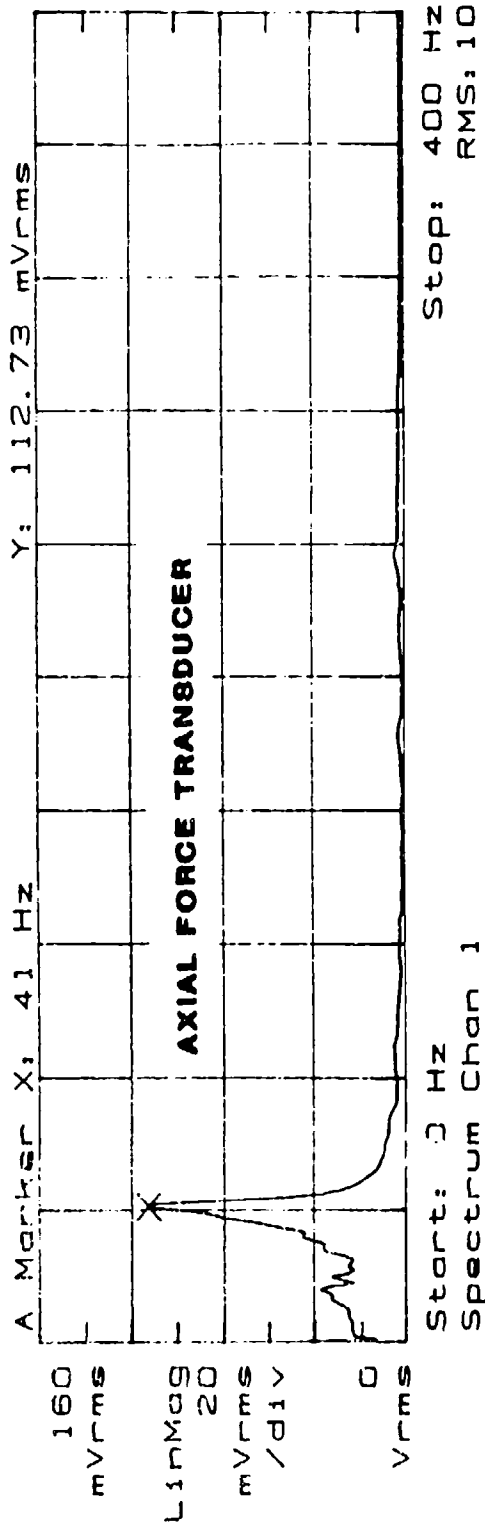
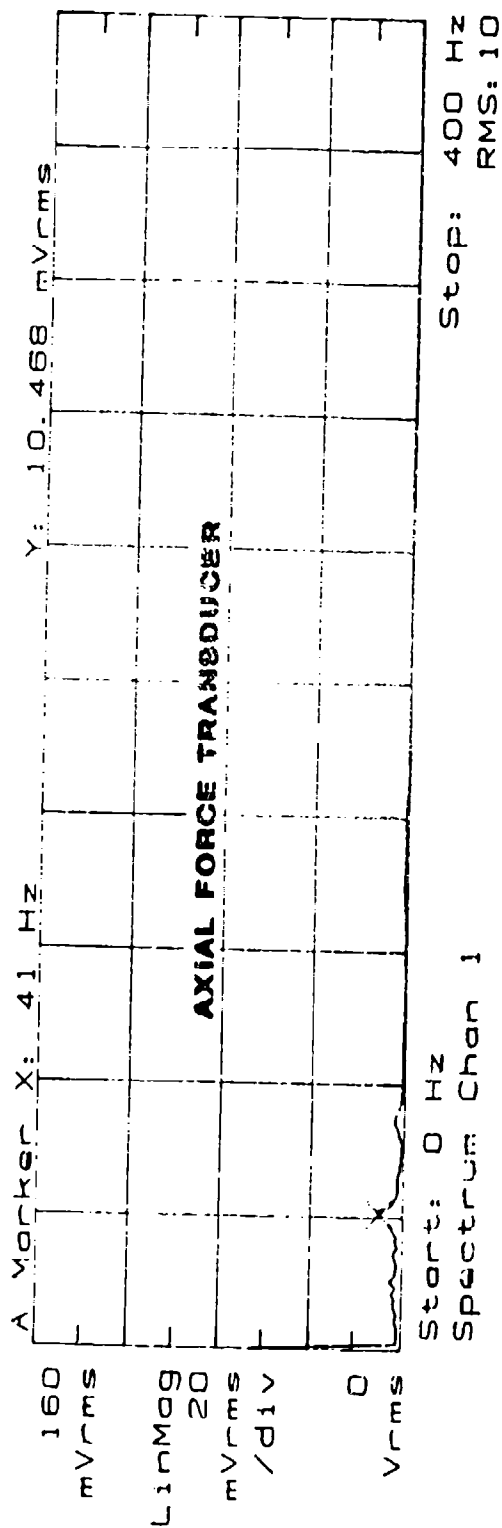


**FIGURE 26 AXIAL FORCE TRANSDUCER
NATURAL FREQUENCY DISTRIBUTION**

REAL-TIME AVG COMPLETE

Src



60

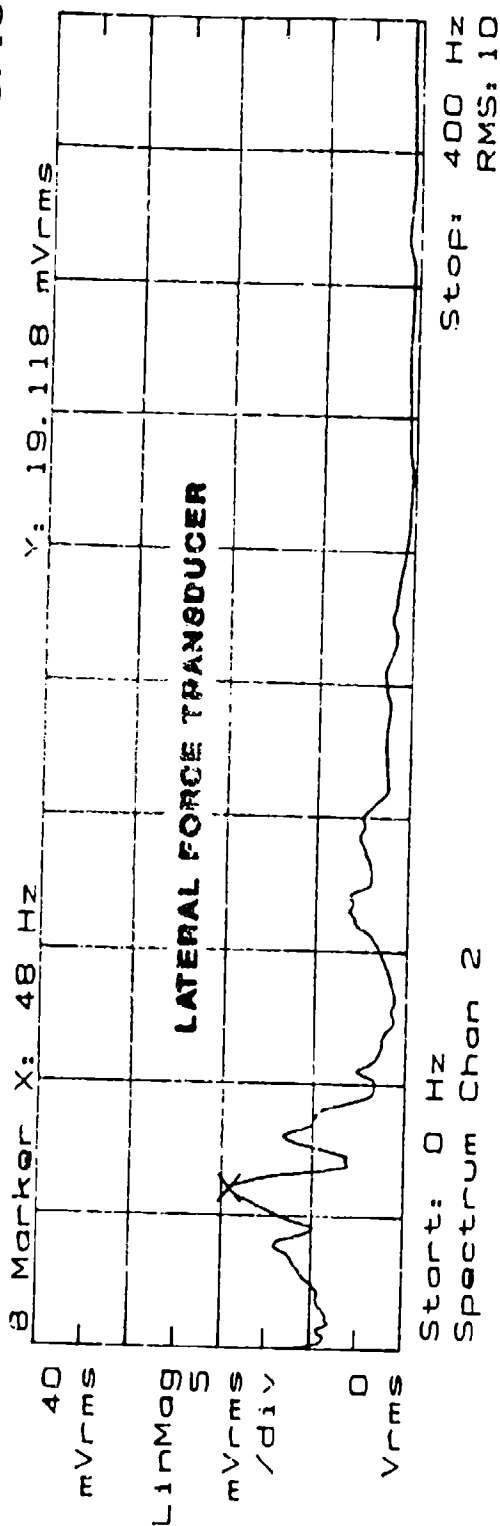
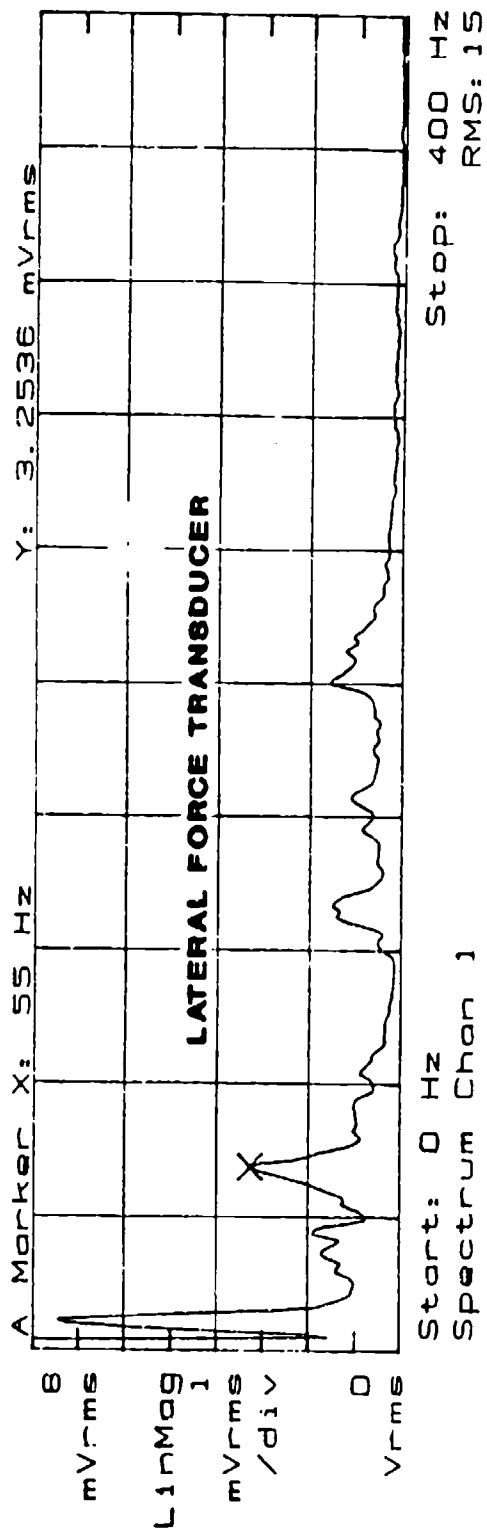
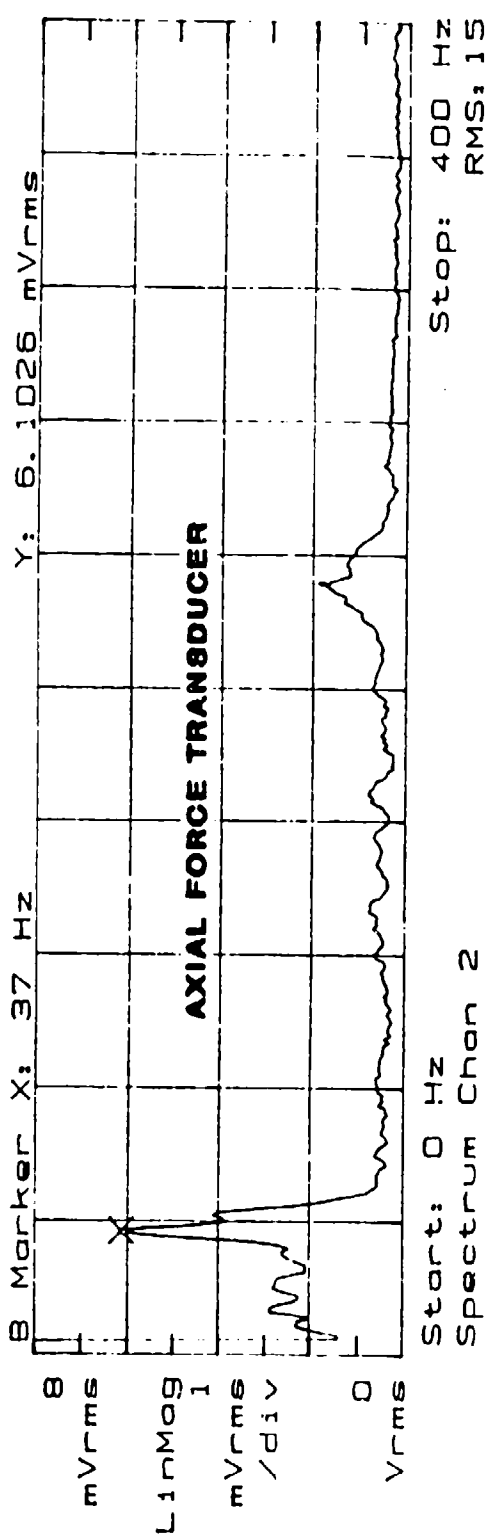


**FIGURE 26 LATERAL FORCE TRANSDUCER
NATURAL FREQUENCY DISTRIBUTION**

REAL-TIME AVG COMPLETE



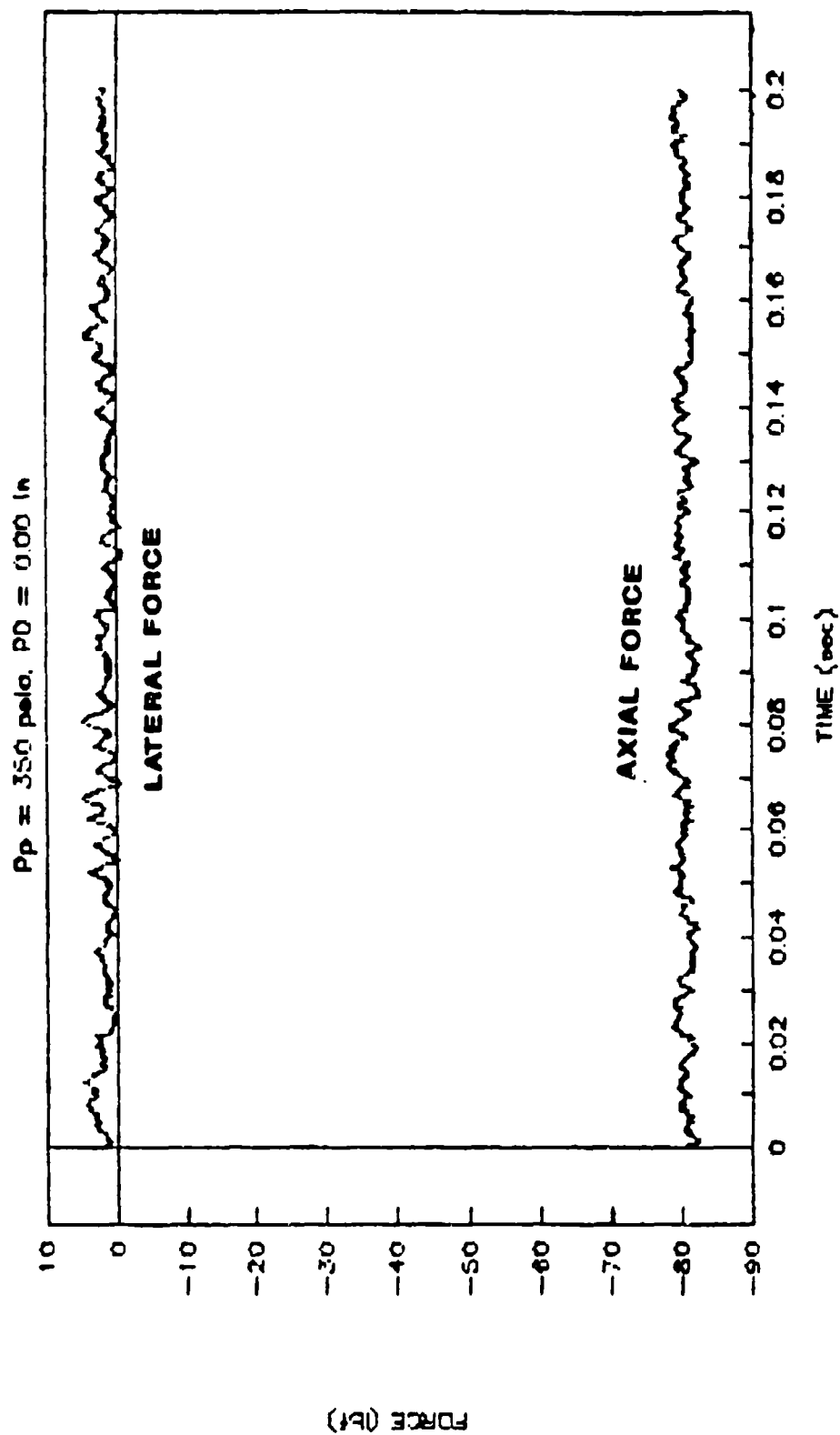
19



**FIGURE 27 STEADY STATE AXIAL FORCE BALANCE
FREQUENCY DISTRIBUTION OF CONFINED JET NOZZLE**

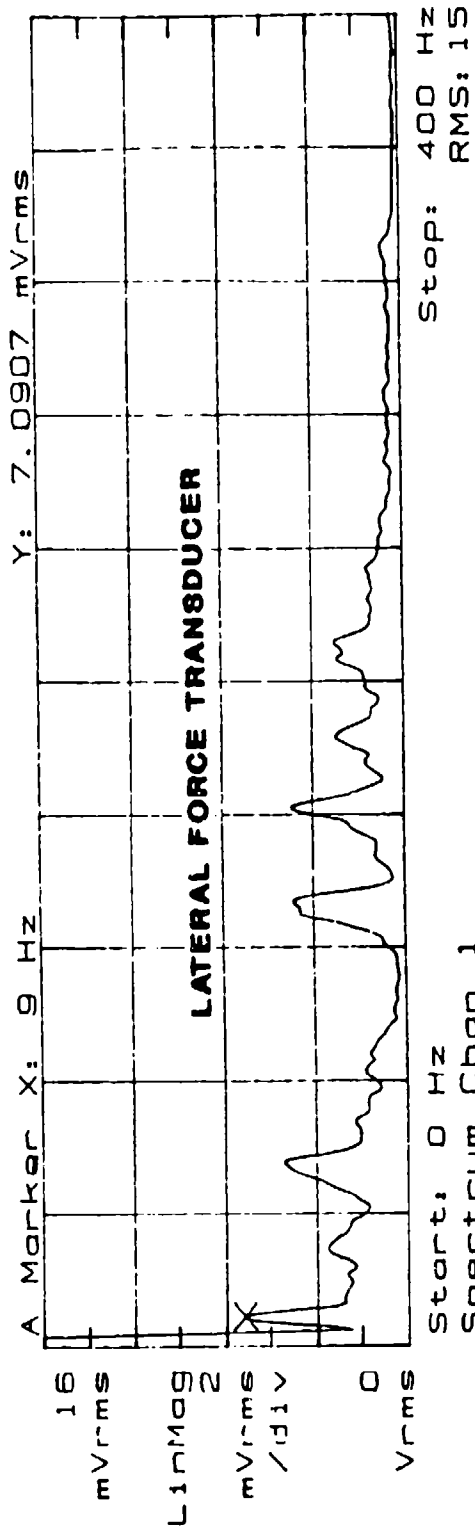
real time data plot of the raw force balance data for a steady state axial confined jet nozzle run is presented in Figure 28. The real time plot shows that during axial operation the force transducers exhibited limited oscillation around a steady value.

Figure 29 shows the frequency spectrum of the force balance and Figure 30 the real time force data for a steady state test run of the confined jet nozzle vectored at $P_p = 350$ psia and pin insertion depth = 0.12 in. The amplitudes of these frequencies and other minor frequencies are amplified during "steady state" vectored operation. Figure 29 shows that frequencies that were not dominant during axial operation are significant during "steady state" vectored operation. This results in a complex signal that tends to oscillate around an average vectored value. This is exhibited by the real time data presented in Figure 30 where the oscillation is much larger in amplitude than for the axial data in Figure 28. It is apparent that the flow within the nozzle is feeding this oscillation and the force balance never really achieves a true steady state value. This required the static values used for the static performance evaluations to be averaged for any meaning. However, due to the natural frequencies of the force balance present the flow oscillation, if any, could not be determined. This made the interpretation of the real time force data as a measure of the transient response somewhat



**FIGURE 28 STEADY STATE AXIAL REAL TIME
FORCE DATA OF CONFINED JET NOZZLE**

REAL-TIME AVG COMPLETE



64

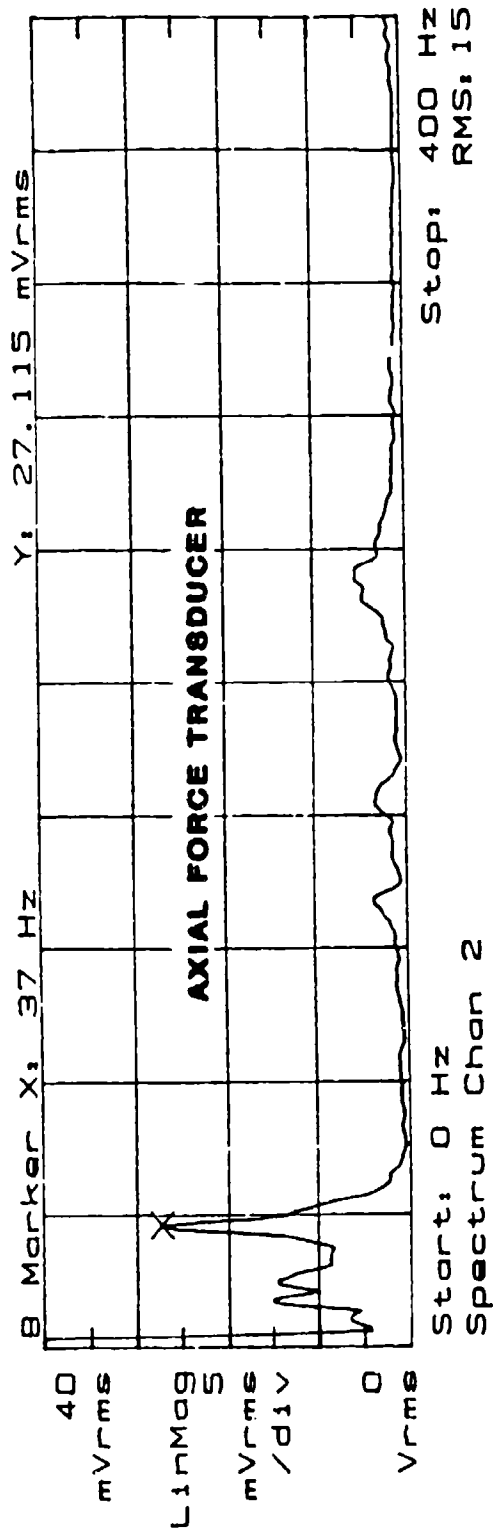


**FIGURE 29 STEADY STATE VECTORED FORCE BALANCE
FREQUENCY DISTRIBUTIONS OF CONFINED JET NOZZLE**

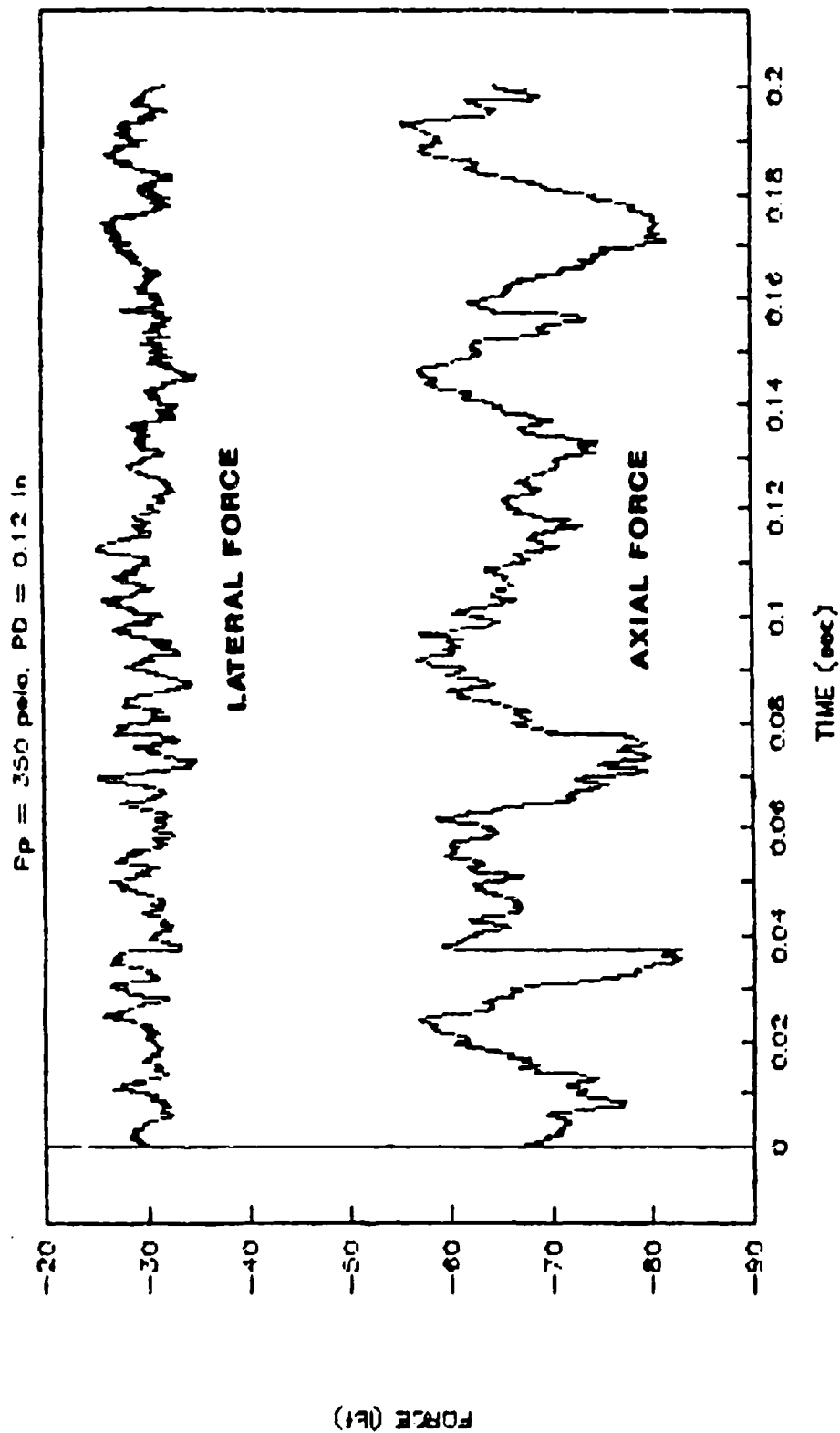


**FIGURE 30 STEADY STATE VECTORED REAL TIME
FORCE DATA OF CONFINED JET NOZZLE**

arbitrary. A possible solution to this problem would be to rebuild the force balance using a light weight metal, like aluminum, to reduce the mass of the force balance. Reducing the mass would raise the resonant frequency of the force balance while retaining the structural integrity to withstand the forces generated by the nozzle. The higher resonant frequency could enable lower frequency flow oscillations to be measured if they exist.

Static Pressure at the Confined Jet Cylinder Wall
(psig) Real Time Data The most meaningful measure of the transient response of the confined jet nozzle to probe thrust vector control was the confined jet cylinder pressure. This measurement was not possible for the conical nozzle as there was no way to mount dynamic pressure transducers to the nozzle; and therefore, only force data could be used. The FFT analysis of the confined jet cylinder pressure signal during vectored and axial operation exhibited no "repeatable" dominant or resonant frequencies over the plenum pressure regime tested ($150 \text{ psia} < P_p < 470 \text{ psia}$). Figure 31 shows the real time response of the confined jet cylinder pressure to a probe thrust vector control insertion disturbance at $P_p = 355 \text{ psia}$ and pin insertion depth = 0.14 in and Figure 32 a pin extraction for the same conditions. Figures 31 and 32 show that the confined jet cylinder pressure signal does oscillate considerably. This again indicates that some

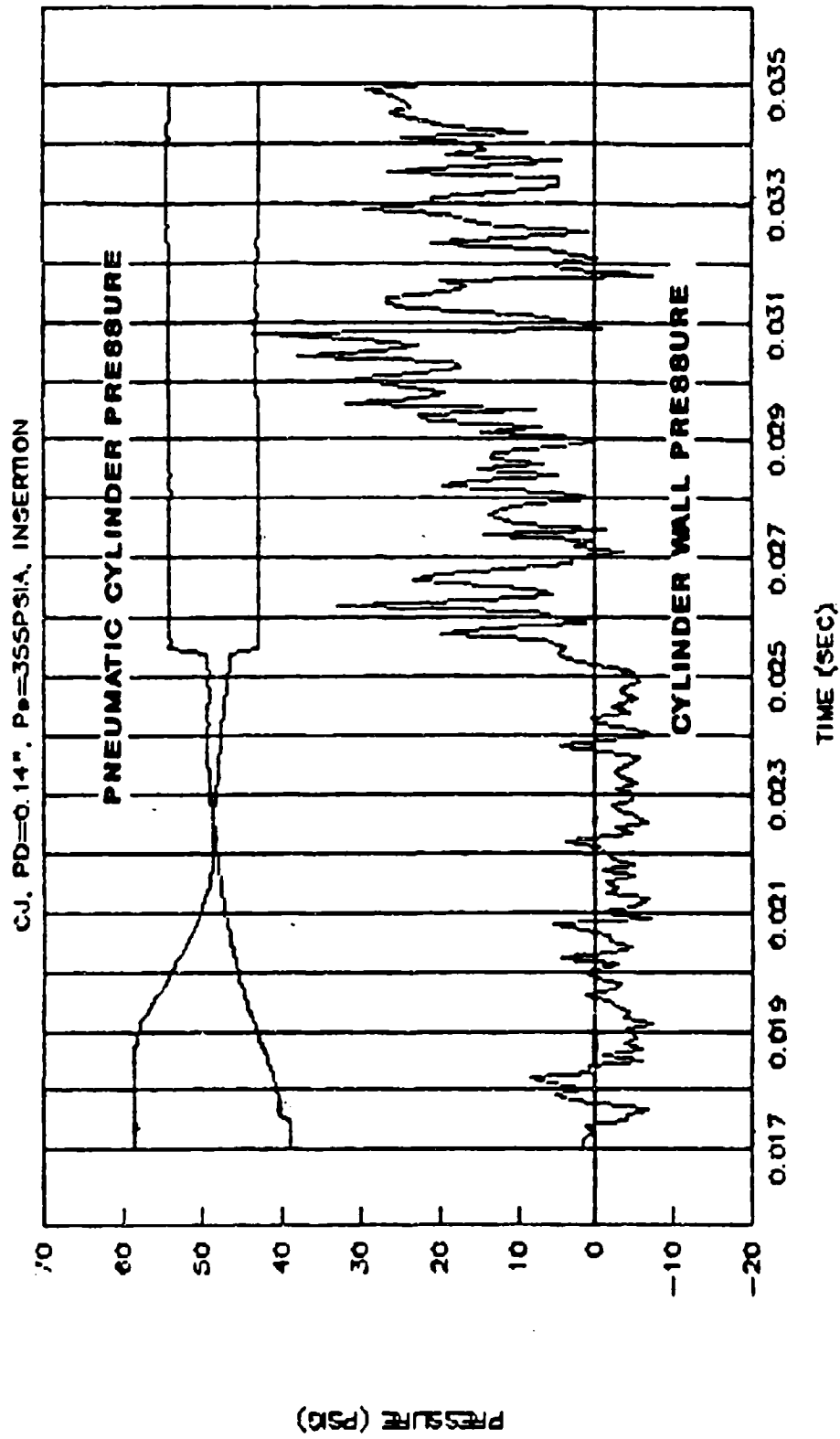


**FIGURE 31 PIN INSERTION REAL TIME CONFINED
JET NOZZLE CYLINDER WALL PRESSURE DATA**

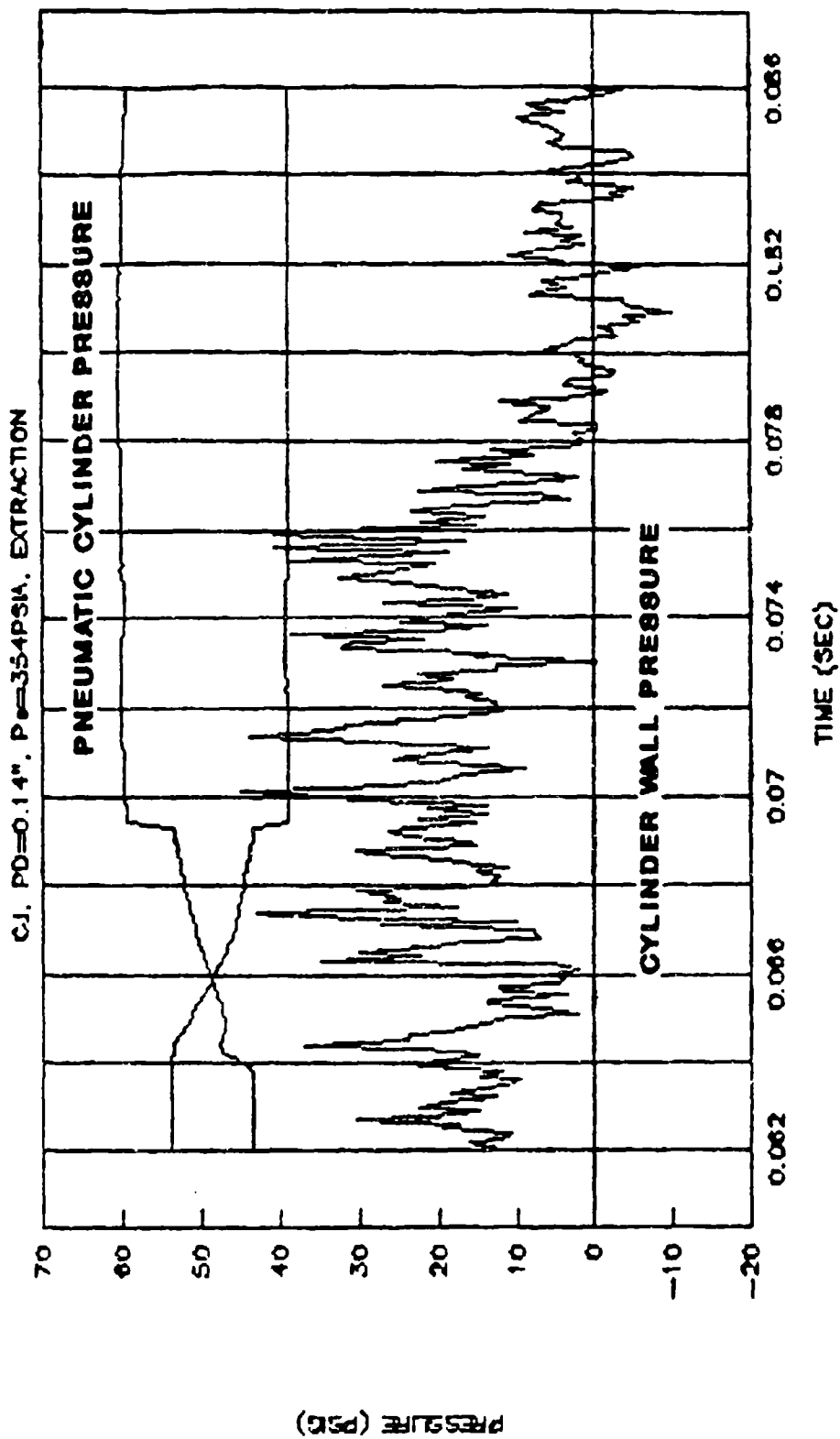


**FIGURE 32 PIN EXTRACTION REAL TIME CONFINED
JET NOZZLE CYLINDER WALL PRESSURE DATA**

unstable flow mechanism is occurring within the nozzle such as vortex shedding from the inserted pin.

The curve at the bottom of the graph indicates the magnitude of the confined jet nozzle cylinder pressure as the nozzle transitions from axial to vectored operation in Figure 31 and the reverse in Figure 32. The curves at the top of the graphs in Figures 31 and 32 represent the secondary pressure applied at both ends of the pneumatic injection cylinder. They basically show when the pin injection device is commanded to vector. The point where the secondary pressure signals step up and down is assumed to be when the pin is fully inserted in or extracted from the flow. Since the transducers on the ends of the pneumatic cylinder were not calibrated it was impossible to tell when the pin actually began to move. The lack of specific information regarding the position of the pin versus time relative to the nozzle wall made it impossible to separate the insertion system from the actual nozzle response.

Insertion System Repeatability

The insertion system response was not repeatable which further limited the transient analysis. This was due to many factors. Possible friction along the insertion bushing caused by actual binding of the pneumatic cylinder along the bushing

and the nozzle wall caused the pin to "stick" and not insert smoothly into the nozzle.

Another problem was the flow impinging on the inserted pin causing it to bind against the downstream nozzle wall and stick. This was seen vividly during conical nozzle tests where the pin took several seconds to extract following the extraction command. The mounting adapter and insertion port diameter were bored out an additional 0.003 in diameter to eliminate this problem. Whether or not this succeeded is inconclusive due to another limitation in the design of the insertion system. This problem was that the design itself was destructive to the pneumatic cylinder. The movement of the pin and collar assembly would compress the bushing on the end of the pneumatic cylinder into the cylinder housing and create additional binding friction within the pneumatic cylinder itself. A possible solution to this problem would be to make a stop that threads onto the pneumatic cylinder to prevent contact of the pin and collar assemblies with the pneumatic cylinder bushing. It may be possible to make this stop as part of the mounting adapter for the nozzle.

D. Probe Thrust Vector Control Transient Response of the Confined Jet Nozzle

The lack of repeatability for the insertion system made interpretation of the transient response difficult. The

insertion system was tested on the confined jet nozzle for four fixed pin insertion depth's: 0.10, 0.14, 0.16 and 0.20 in. This range of pin insertion depth's was selected because it gave the most consistent vector time response for the confined jet nozzle. Smaller pin insertion depths provided inconsistent vector time responses. Despite the limitations of the instrumentation, generalizations about the transient response can be inferred from the data.

Insertion Response: The vector time response of the confined jet nozzle, as might be expected, was dependent on pin insertion depth. The larger pin insertion depth's tended to exhibit a quicker rise in confined jet cylinder pressure than for the smaller pin insertion depth's. The real time force data revealed that at some of the smaller pin insertion depth's the nozzle might attach to the pin for a period of time before deflecting to the other side of the confined jet nozzle. Figure 33 shows an example of this. The apparent reason for this is that it takes longer for the bow shock created by the smaller pin insertion depth's to create a disturbance large enough to vector the axial core flow. At larger pin insertion depth's the vectored confined jet cylinder pressure rise lagged the Pneumatic cylinder pressure step by only a few milliseconds.

The response of the confined jet nozzle also depended on P_p . In general the confined jet nozzle responded quicker

VC-1, PD=0.10", P=351PSIA, INSERTION

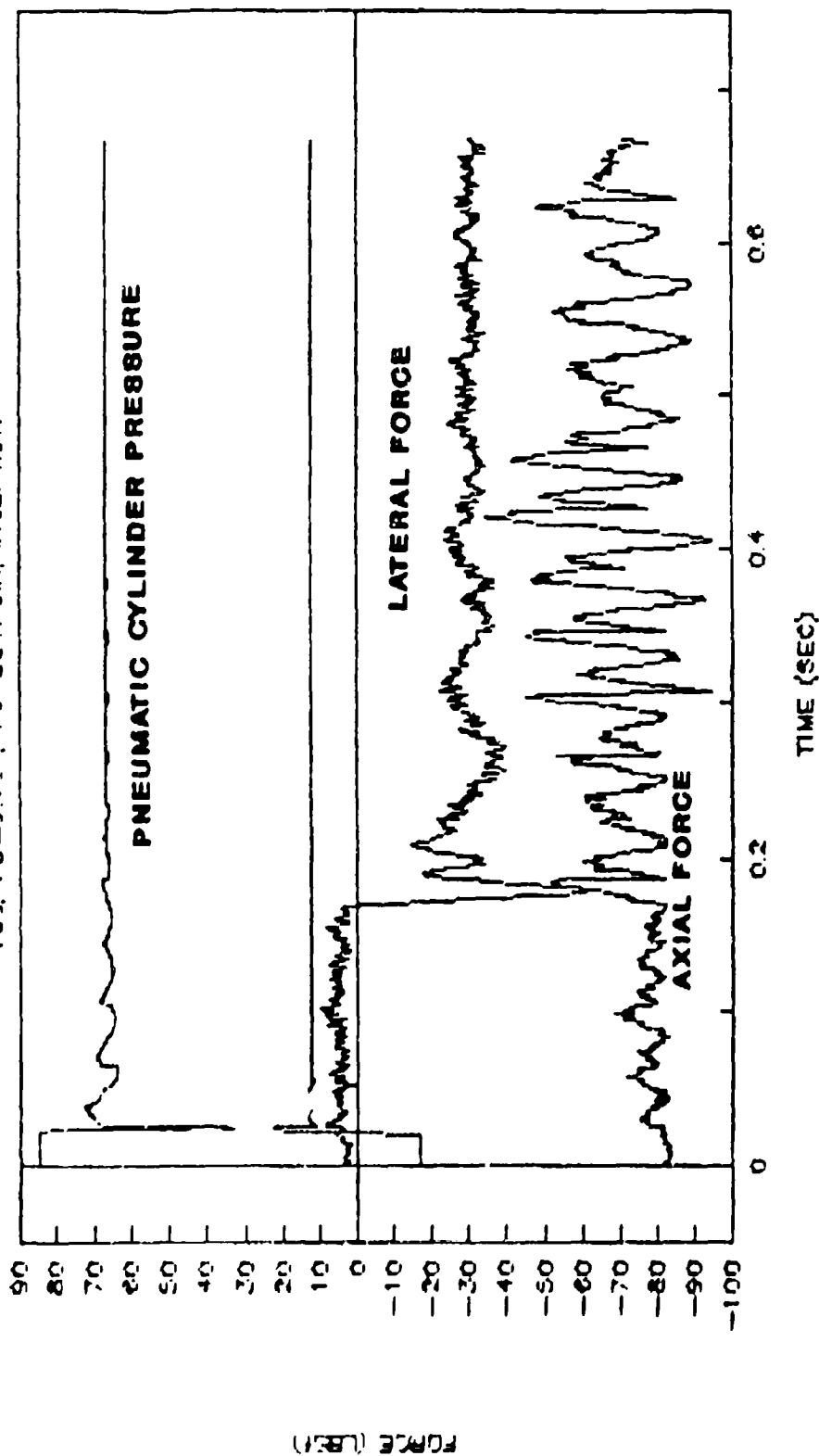
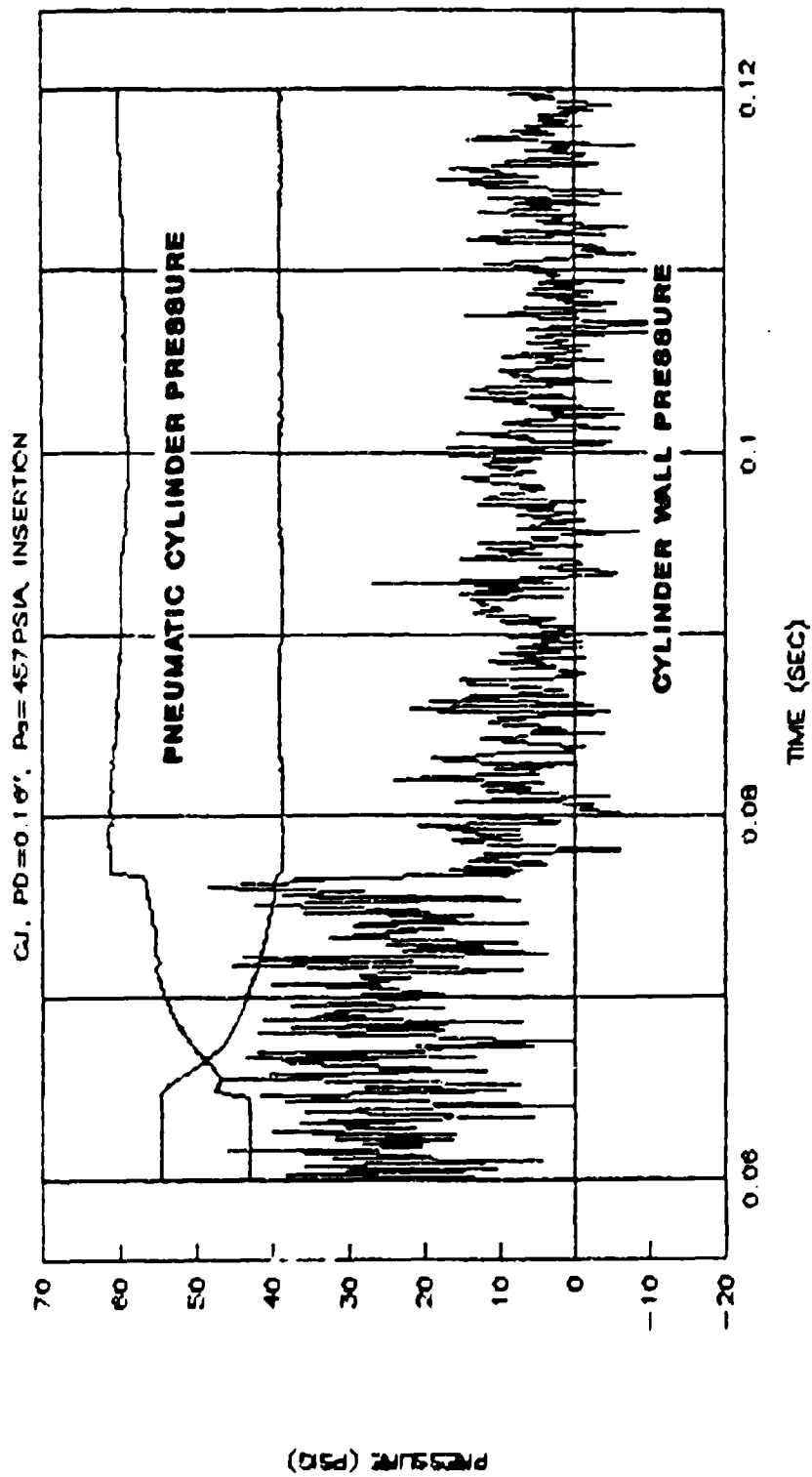


FIGURE 33 PIN INSERTION REAL TIME FORCE DATA/
FLOW ATTACHMENT TO PIN

at the high P_p 's. This is probably due to the higher density and static wall pressure at the insertion ports at higher plenum pressures. The probe thrust vector control disturbance would then be stronger as the bow shock was stronger and affect the axial core flow faster. The increased strength of the bow shock penetrates into the core flow faster. The overall response of the pin insertion system and the confined jet nozzle was on the order of 10-15 milliseconds. This is the same order of magnitude for the vector time response of the confined jet nozzle to secondary injection thrust vector control found by Friddell(3).

Extraction Response The confined jet nozzle did not "unvector" in the same manner each time. In one mode (Figure 34) the confined jet cylinder pressure would drop abruptly to the axial value a given period after the pin was extracted. However, this ranged in value from a couple milliseconds up to 20 milliseconds. Another mode (Figure 35) was where the confined jet cylinder pressure would drop to an intermediate value before dropping to the axial value. This is similar to the delays found by Friddell (3) and Lerup (4). A third mode (Figure 36) was where the confined jet nozzle switched abruptly from the vectored confined jet cylinder pressure value to the axial confined jet cylinder pressure value and back to the vectored confined jet cylinder pressure value before returning to the stable axial confined jet cylinder



**FIGURE 34 PIN EXTRACTION, CYLINDER WALL
PRESSURE DATA/ABRUPT TRANSITION**

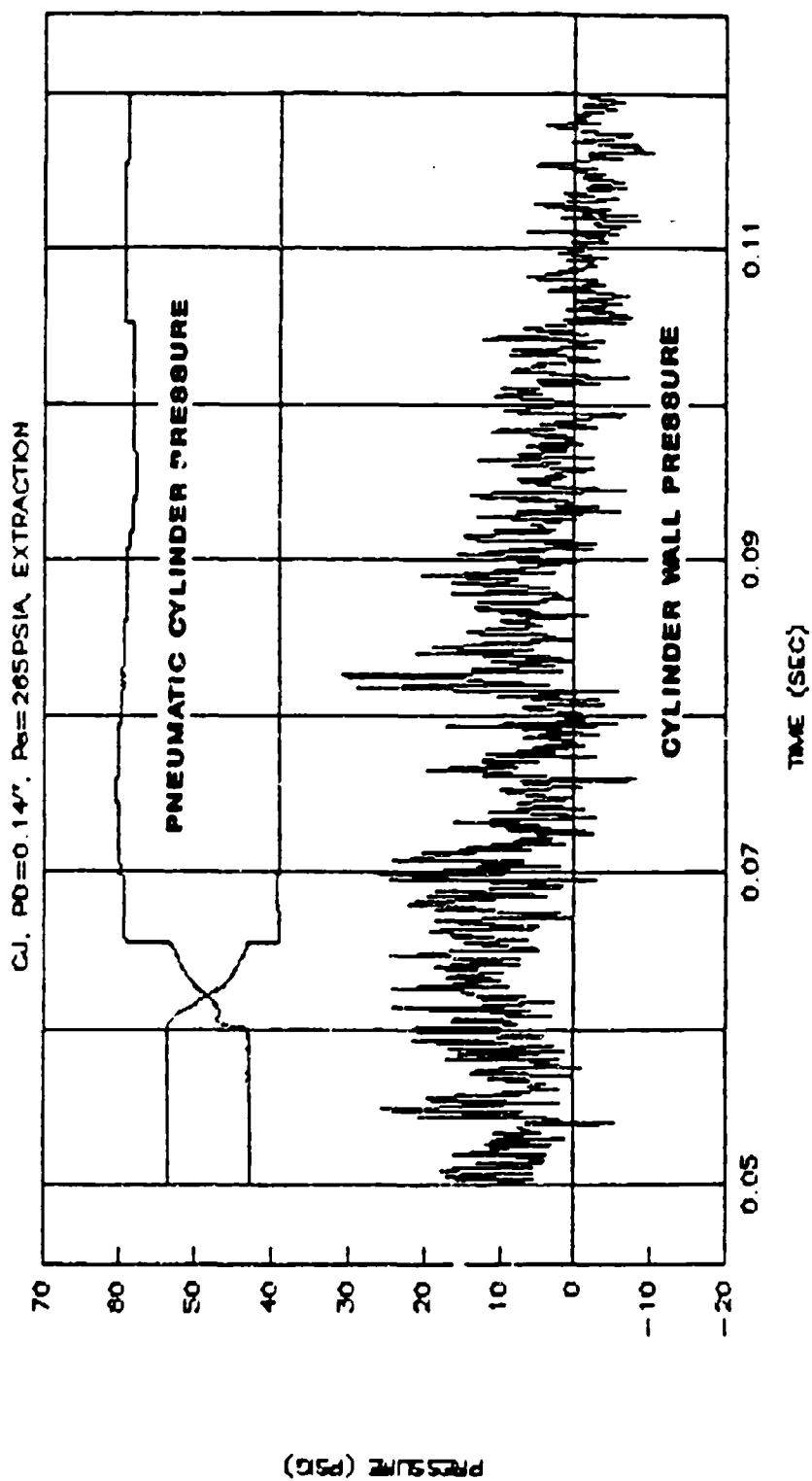


**FIGURE 36 PIN EXTRACTION, CYLINDER WALL
PRESSURE DATA/TRANSITION WITH HISTORIS**

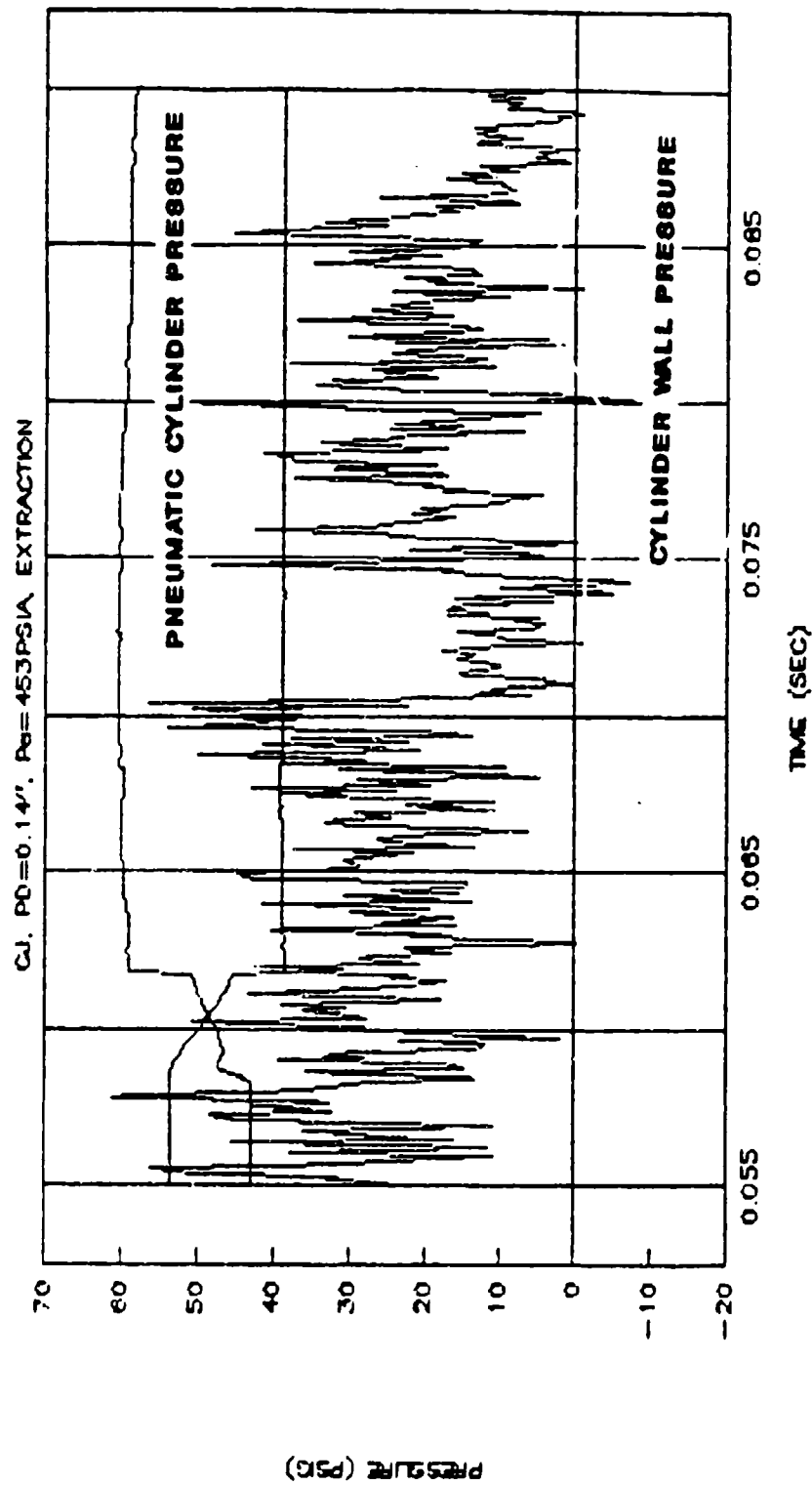


**FIGURE 38 PIN EXTRACTION, CYLINDER WALL
PRESSURE DATA/UNSTABLE TRANSITION**

pressure value. The transient of the pin insertion system and the confined jet nozzle varied from 10-20 milliseconds. The extraction response in general did not depend on pin insertion depth but on the flow mechanisms of the confined jet nozzle and the performance of the extraction system.

E. Multiple Pins in the Confined Jet Nozzle

Herup (4) found that the use of two pins inserted into the confined jet nozzle 90 deg apart during static tests produced a flow attachment or "vector angle" between the two pins. He found that the resulting vector angle between the pins was unpredictable. In static tests the flow would attach in either of two ways: the flow would vector in the same manner as the one pin case to either pin or the flow would vector to an intermediate angle between the pins(4:82). These vectored conditions were stable once the confined jet nozzle vectored.

Dynamic tests with multiple pins were performed using the pin insertion/extraction system. During these tests axial flow was established in the confined jet nozzle and one pin was inserted into the flow to vector the nozzle in the plane of the force balance. Once vectored flow was established the second pin 90 deg from the first was inserted. The data indicated no significant changes in the original vectored steady state force balance measurements of the confined jet

nozzle and no change in flow direction indicated on the flow visualization grid at the nozzle exit. Once the first pin was extracted the flow vectored from the second pin causing the vector angle to switch 90 deg.

Dynamic tests were also performed where two pins 90 deg apart were commanded to insert at the same time. The control system sent the commands to the solenoid valves at the same time. However, due to the dynamics of the pin insertion/extraction system one pin would always lead the other in disturbing the nozzle flow. The confined jet nozzle was found to vector from whichever pin created the first disturbance. This is where the performance of the pin probe thrust vector control differs significantly from the results obtained for secondary injection in the confined jet nozzle. Herup found that the confined jet nozzle would vector to intermediate angles between fluid injection ports at 90 deg angles (4:63). This is due to the interaction of the primary nozzle flow and the secondary injection flow. This interaction is highly dependent upon the conditions of the secondary injection fluid flow relative to the primary nozzle flow (3). This is the primary difference in the internal flow mechanism between secondary injection thrust vector control and pin probe thrust vector control. The only action in probe thrust vector control is the physical or mechanical deflection of the primary flow. Secondary injection thrust vector

control, in addition to the bow shock deflecting the core flow, has mass addition occurring at the wall.

It may be possible to vector the confined jet nozzle with two pins depending on the insertion location and the size of the pin. The nozzle is very responsive or sensitive to disturbances. It has been found during this investigation and previous work that small burrs at the insertion port can significantly change the stable axial operation of the nozzle. The effect of pin diameter versus nozzle geometry is unknown. It may be possible to control the size of the separation region within the nozzle. This could be accomplished by varying the pin diameter and location relative to the throat of the nozzle. This could enable flow deflections between multiple pins inserted in the nozzle.

F. Probe Thrust Vector Control Transient Response of the Conical Nozzle

The pin insertion/extraction system was unable to reliably vector the conical nozzle due to the insertion system binding problems discussed earlier. Due to the geometry of the nozzle and insertion device the only pin insertion depth tested was 0.38 in. In order to dynamically test each pin depth evaluated previously in static tests, new pin attachments for each pin depth were required. The pin depth of 0.38 in was selected because it provided the best response

in static tests (see Figure 20). This large pin insertion depth was exposed to the nozzle flow causing binding between the cylinder and the wall of the nozzle. It was possible to vector the conical nozzle from axial flow condition with pin insertion. However, the pin insertion and extraction was not repeatable due to the binding noted earlier. The binding effect was most pronounced for extractions. This effectively delayed the transition from vectored to axial flow. The conical nozzle could be made to vector to the static test values using the pin insertion system and would return to the axial values once the pin was extracted. The vector time response observed was dominated by the delays of the probe thrust vector control mechanism making observations of the conical nozzle flow response impossible.

V. Conclusions

A. Objective #1:

The static wall pressure distribution and axial forces of the conical nozzle and confined jet nozzle were evaluated in axial operation and found to agree with the results of previous test using the same nozzles. The confined jet nozzle produced 75%-90% of the axial force produced by the conical nozzle over the same stagnation pressure range ($150 \text{ psia} < P_p < 470 \text{ psia}$). The separation point was located using the static wall pressure distribution for both configurations to establish the flow condition within the diverging nozzle over the pressure ranges tested.

The flow condition around the insertion port was found to be a primary factor for pin probe thrust vector control performance. The conical nozzle would not vector successfully for most of the pin insertion depths tested over the pressure ranges where the axial flow separation point was near the insertion port location ($150 \text{ psia} < P_p < 270 \text{ psia}$). Above this pressure range the conical nozzle produced stable vectored flow for most of the pin insertion depths tested. Pin insertion depth and plenum pressure were seen as the primary factors in probe thrust vector control performance for the conical nozzle. Pin probe thrust vector control is a viable flow vectoring mechanism at plenum pressures that

produce fully expanded flow downstream of the insertion port in the conical nozzle. Lateral forces of approximately 12% of the axial force were produced with pin insertion depth = 0.375 in at $P_p > 270$ psia.

Pin probe thrust vector control is a viable flow vectoring mechanism for the confined jet nozzle. The separation point was found to be downstream of the insertion port for the pressure range tested. All the pin insertion depths used in "static" test produced vectored flow in the confined jet nozzle. The pin insertion depths used in the confined jet were much smaller than the pin insertion depths that produced vectored flow in the conical nozzle. Once the confined jet nozzle was vectored the lateral forces produced by the nozzle were not significantly different over the range of pin insertion depths tested. The confined jet produced lateral forces of 45-60% of the vectored axial force over the plenum pressure range tested.

The airfoils were tested in both configurations and found to be as effective as the pins in creating vectored flow within the plane of the disturbance. The airfoils were able to vector both configurations in the same manner as pin probe thrust vector control when the airfoil was rotated 90 deg from the centerline. This presented the same disturbance as a pin inserted the same distance and produced similar lateral forces. Steady axial performance in both configurations was

not possible with the airfoils inserted at zero angle of attack. When the airfoils were at zero angle of attack, the flow would vector away from the pin that created the largest disturbance.

B. Objective #2:

The data obtained for both the conical nozzle and confined jet nozzle compared reasonably with previous tests using the same nozzle configurations using secondary injection thrust vector control as the vectoring mechanism. The conical nozzle produced limited lateral forces of 12% of axial force using probe thrust vector control. Friddell found secondary injection thrust vector control in the conical nozzle produced lateral forces of 15% of the axial force. Pin probe thrust vector control can produce similar lateral force as secondary injection thrust vector control in the conical nozzle.

One of the problems associated with probe thrust vector control in a conical nozzle is the large pin insertion depths required to obtain significant lateral forces. In this investigation the pin was inserted between 30-80% of the distance from the nozzle wall to the nozzle centerline to produce these forces. This would require significant cooling for the pin in a typical rocket nozzle to prevent ablation and consequently loss of probe thrust vector control performance.

The confined jet nozzle also produced similar lateral forces with pin thrust vector control to those produced in

previous tests using secondary injection thrust vector control. The confined jet nozzle produced lateral forces of approximately 45% of the axial force using pin thrust vector control. Herup found that using secondary injection thrust vector control lateral forces of 50% of the axial force were possible. The pin insertion depths required to produce these forces were roughly 30% of the distance from the nozzle wall to the nozzle centerline. This is significantly less than the pin insertion depth required in the conical nozzle.

C. Objective #3:

Pin probe thrust vector control was effective in dynamically vectoring both configurations from axial flow to vectored flow. The primary factors determining the effectiveness of pin probe thrust vector control were: the flow condition near the insertion port and the pin insertion depth (pin insertion depth). When the flow was supersonic and fully expanded at the insertion port pin probe thrust vector control was most consistent and reliable. Pin insertion depth was a factor in how quickly the pin disturbance perturbed the nozzle flow and deflected it to a vectored condition. The extraction response did not depend on pin insertion depth but on the flow mechanisms of the confined jet nozzle and the performance of the extraction system. In general probe thrust vector control exhibited vector time transients on the order of 10-20ms for the

transition from axial to vectored flow and vectored to axial flow.

The pin insertion/extraction system used in this study did not allow the pin position relative to the nozzle wall to be known versus time. This prevented the separation of the insertion system dynamics from the flow dynamics of the nozzles. Therefore, the vector time transients observed were for the vectoring mechanism and the nozzle as a whole system.

D. Objective #4:

The transients observed in the confined jet nozzle were of the same magnitude as observed by Herup and Friddell in studies using secondary injection thrust vector control on the same confined jet nozzle configuration. The transient from vectored to axial flow by the confined jet nozzle exhibited similar phenomena as observed by Herup and Friddell using secondary injection thrust vector control. The confined jet nozzle appears to have a complicated flow process during this transition. The complexity of the flow mechanisms involved were exhibited by the confined jet cylinder pressure response. The confined jet cylinder pressure was observed to respond in three ways: remain vectored for 10-20ms after the pin was extracted, return immediately to the axial value when the pin was extracted, and oscillate once between axial and vectored values before stabilizing at the axial value. The first mode of transition could be explained by coupling with

the extraction system. The last mode of transition where the confined jet nozzle cylinder wall pressure fluctuates between axial forces indicate that the fluid flow within the nozzle is very complex.

VI. Recommendations

1. The addition of the Z-286 PC with the A/D board enable recording of large amounts of dynamic force and pressure data within a short time making transient evaluations possible.

This streamlines the data reduction process considerably by converting digital data directly to ASCII files for data reduction. The A/D board needs to be upgraded to a six channel board to allow force, pressure, and control inputs to be recorded simultaneously for each run.

2. The nozzle configuration should be scaled down to enable testing of the conical nozzle at fully expanded flow conditions where nozzles are generally operated.

3. The pin insertion mechanism needs to be modified to allow accurate measurement of pin position vs time relative to the nozzle wall. The pin insertion system also needs to be improved to prevent binding during insertion.

4. The force balance needs to be replaced with a higher frequency balance to enable evaluation of the frequency distribution of the nozzle response. This would evaluate the low frequency response of the nozzles to determine if a repeatable shedding frequency exists during vectored operation.

Bibliography

1. Covalleri, R., Tiarn, W., and Readey, H. "Thrust Vector Control Using Moveable Probes" (Paper No. AIAA 90-0562). AIAA 28th Aerospace Sciences Meeting. Reno, NV, January 1990.
2. Fitzgerald, R. E., and Kampe, R. F. "Boundary Layer TVC for Missile Applications" (Paper No. AIAA 83-1153). AIAA/SAE/ASME 19th Joint Propulsion Conference. Seattle, WA, June 1990.
3. Friddell, Jerold H. Steady State and Dynamic Behavior of an Axisymmetric Confined Jet Thrust Vector Control Nozzle. MS Thesis. Air Force Institute of Technology (AU), Wright-Patterson AFB OH, December 1988.
4. Herup, Eric J. Confined Jet Thrust Vector Control Nozzle Studies. MS Thesis. Air Force Institute of Technology (AU), Wright-Patterson AFB OH, December 1989.
5. Porzio, Anthony J. Characteristics of a Confined Jet Thrust Vector Control Nozzle. MS thesis. Air Force Institute of Technology (AU), Wright-Patterson AFB OH, December 1984.
6. Qua Tech Inc. 12 Bit "Analog to Digital Conversion Board Users Manual." 478 E. Exchange St. Akron OH 44304. Undated.
7. Ryan, Robert W. Flow Response of Axisymmetric Confined Jet Thrust Vector Control Nozzle. MS Thesis. Air Force Institute of Technology (AU), Wright-Patterson AFB OH, December 1987.

Vita

Curtis R. Amble was born in Edina, Minnesota on 7 January 1960. He graduated from the University of Minnesota's Institute of Technology in 1982 with a Bachelor of Science in Mechanical Engineering. He graduated from Officer's Training School and was assigned to Arnold Engineering Development Center where he was a re-entry systems test manager. He was then assigned to Aeronautical Systems Division where he served as the B1-B defensive systems test manager. He entered the Air Force Institute of Technology Graduate Astronautical Engineering Program in May 1990.

Permanent Address: 6108 Kellogg Ave.

Edina, MN 55424

REPORT DOCUMENTATION PAGE

Form Approved
OMB No 0704-0186

Public reporting burden for this document is estimated to be 1 hour per document, including the time for reviewing instructions, searching existing data sources, gathering and maintaining the data needed, completing and reviewing the collection of information, and reviewing and approving the collection of information. Send comments regarding this burden estimate or any other aspect of this collection of information, including suggestions for reducing the burden, to Washington Headquarters Services, Directorate for Information Operations and Reports, 1215 Jefferson Davis Highway, Suite 1204, Arlington, VA 22202-4302, and to the Office of Management and Budget, Paperwork Reduction Project (0704-0186), Washington, DC 20503.

1. AGENCY USE ONLY (Leave blank)		2. REPORT DATE DEC 91	3. REPORT TYPE AND DATES COVERED MS THESIS	
4. TITLE AND SUBTITLE THRUST VECTOR CONTROL OF AN OVEREXPANDED SUPERSONIC NOZZLE USING PIN INSERTION AND ROTATING AIRFOILS			5. FUNDING NUMBERS	
6. AUTHOR(S) CURTIS R. AMBLE, Capt, USAF				
7. PERFORMING ORGANIZATION NAME(S) AND ADDRESS(ES) SCHOOL OF ENGINEERING AIR FORCE INSTITUTE OF TECHNOLOGY WRIGHT-PATTERSON AFB OH 45433			8. PERFORMING ORGANIZATION REPORT NUMBER AFIT/GA/ENY/91D-12	
9. SPONSORING MONITORING AGENCY NAME(S) AND ADDRESS(ES) DAVID R. SELEGAN WL/FIM WRIGHT-PATTERSON AFB OH 45433			10. SPONSORING MONITORING AGENCY REPORT NUMBER	
11. SUPPLEMENTARY NOTES				
12a. DISTRIBUTION AVAILABILITY STATEMENT UNLIMITED DISTRIBUTION			12b. DISTRIBUTION CODE A	
13. ABSTRACT (Maximum 200 words) An experimental study of probe thrust vector control of overexpanded supersonic flow in nozzles using moveable probes as the vectoring mechanism is presented. Two types of moveable probes were used. The first inserted cylindrical probes through the wall of the nozzle to set depths relative to the nozzle wall. The second used rotating airfoils, inserted within the nozzle flow, rotated to various angles of attack relative to the nozzle centerline. The effectiveness of these probe thrust vector control mechanisms were investigated for a confined jet and conical nozzle. The objective of this study was to evaluate performance and transient characteristics of these probe thrust vector control mechanisms. Axial force, lateral force, and static nozzle wall pressure distribution data were measured for axial and vectored operation for each nozzle configuration. Parameters that were varied included primary stagnation pressure, cylinder insertion depth, airfoil insertion depth, and angle of attack.				
14. SUBJECT TERMS THRUST VECTOR, CONFINED JET NOZZLE, CONICAL NOZZLE, MOVEABLE PROBES			15. NUMBER OF PAGES 98	
			16. PRICE CODE	
17. SECURITY CLASSIFICATION OF REPORT UNCLASSIFIED	18. SECURITY CLASSIFICATION OF THIS PAGE UNCLASSIFIED	19. SECURITY CLASSIFICATION OF ABSTRACT UNCLASSIFIED	20. LIMITATION OF ABSTRACT UNLIMITED	